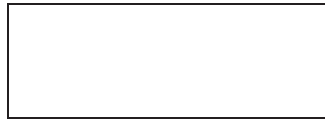




**A 'Boscastle-type' quasi-stationary convective system over
the UK Southwest Peninsula**

Journal:	<i>QJRMS</i>
Manuscript ID:	QJ-12-0205
Wiley - Manuscript type:	Research Article
Date Submitted by the Author:	05-Sep-2012
Complete List of Authors:	Warren, Robert; University of Reading, Department of Meteorology Kirshbaum, Daniel; McGill University, Department of Atmospheric and Oceanic Sciences Plant, Robert; University of Reading, Department of Meteorology Lean, Humphrey; Met Office, MetOffice@Reading
Keywords:	heavy precipitation, convergence line, sea breeze, Unified Model



A 'Boscastle-type' quasi-stationary convective system over the UK Southwest Peninsula

R. A. Warren^{a*}, D. J. Kirshbaum^b, R. S. Plant^a, H. W. Lean^c

^a*Department of Meteorology, University of Reading, Reading, UK*

^b*Department of Atmospheric and Oceanic Sciences, McGill University, Montreal, Quebec, Canada*

^c*MetOffice@Reading, University of Reading, Reading, UK*

*Correspondence to: R. A. Warren, Department of Meteorology, University of Reading, Earley Gate, PO Box 243,
Reading, RG6 6BB, UK. E-mail: r.a.warren@pgr.reading.ac.uk

An investigation is presented of a quasi-stationary convective system (QSCS) which occurred over the UK Southwest Peninsula on 21 July 2010. This system was remarkably similar in its location and structure to one which caused devastating flash flooding in the coastal village of Boscastle, Cornwall on 16 August 2004. However, in the 2010 case rainfall accumulations were around four times smaller and no flooding was recorded. The more extreme nature of the Boscastle case is shown to be related to three factors: (1) higher rain rates, associated with a warmer and moister tropospheric column and deeper convective clouds; (2) a more stationary system, due to slower evolution of the large-scale flow; and (3) distribution of the heaviest precipitation over fewer river catchments. Overall, however, the synoptic setting of the two events was broadly similar, suggesting that such conditions favour the development of QSCSs over the Southwest Peninsula.

A numerical simulation of the July 2010 event was performed using a 1.5-km grid length configuration of the Met Office Unified Model. This reveals that convection was repeatedly initiated through lifting of low-level air parcels along a quasi-stationary coastal convergence line. Sensitivity tests are used to show that this convergence line was a sea breeze front which temporarily stalled along the coastline due to the retarding influence of an offshore-directed background wind component. Several deficiencies are noted in the 1.5-km model's representation of the storm system, including delayed convective initiation; however, significant improvements are observed when the grid length is reduced to 500 m. These result in part from an improved representation of the convergence line, which enhances the associated low-level ascent allowing air parcels to more readily reach their level of free convection. The implications of this finding for forecasting convective precipitation are discussed.

Copyright © 0000 Royal Meteorological Society

Key Words: heavy precipitation; convergence line; sea breeze; Unified Model

Received ...

Citation: ...

1. Introduction

The so-called First Law of Quantitative Precipitation Forecasting, attributed to C. F. Chappell, states that ‘the heaviest precipitation occurs where the rainfall rate is the highest for the longest time’ (Doswell *et al.* 1996). Ordinary single-cell thunderstorms may produce heavy rainfall, but they rarely last long enough to give significant localised accumulations. On the other hand, if multiple convective cells repeatedly pass over the same area in rapid succession, extreme rainfall totals can occur. This process may be associated with ‘back-building’ mesoscale convective systems (MCSs) in which the upstream development of new cells matches the system’s downstream translation speed (Chappell 1986; Schumacher and Johnson 2005). It may also be associated with repeated topographically forced initiation of cells over the same location (e.g. Maddox *et al.* 1978). Both situations result in a quasi-stationary convective system (QSCS) which can locally produce extreme rainfall accumulations.* Depending on the intensity of the rain produced, the duration of the system, the distribution of rainfall over different drainage basins, and the characteristics of these drainage basins (e.g. antecedent moisture, slope, soil porosity, vegetation cover) flash flooding may occur (Davis 2001). Worldwide, many severe flash floods have been attributed to QSCSs (e.g. Maddox *et al.* 1978; Shepherd and Colquhoun 1985; Petersen *et al.* 1999; Romero *et al.* 2000; Golding *et al.* 2005; Ducrocq *et al.* 2008; Zhang and Zhang 2012).

For a storm system to become quasi-stationary, local conditions must remain conducive to the development of deep, moist convection (DMC) for an extended period of time. Thus, there must be a continuous supply of moisture and instability, and a persistent mechanism to lift parcels of air to their level of free convection (LFC). Typically, moisture and instability are provided by the local surface

*Heavy localised precipitation may also be associated with non-stationary linear MCSs where cell motion is approximately parallel to the convective line (the ‘training line, adjoining stratiform’ classification of Schumacher and Johnson 2005).

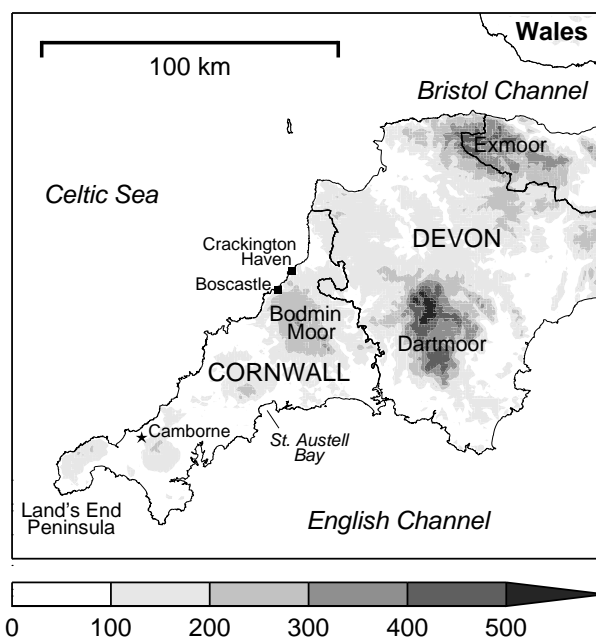


Figure 1. Map of the UK Southwest Peninsula showing orography height (metres, shading; $\Delta x = 500$ m) and locations mentioned in the text. Thick contours mark county borders with county names shown in upper case. See Figure 7 for location within the UK.

fluxes of heat and water vapour, and/or synoptic-scale circulations which can be readily identified in relatively coarse observational and model analyses (Maddox *et al.* 1979). In contrast, the mechanisms for storm initiation frequently occur at the mesoscale or storm-scale (Doswell 1987). These mechanisms include buoyancy-driven circulations (thermals, horizontal convective rolls), boundary layer convergence zones (associated with fronts, drylines, convective outflow boundaries, roughness gradients, differential surface heating, and flow blocking and deflection by topography), forced topographic ascent, gravity waves, and secondary circulations associated with upper-tropospheric jet streaks. In addition to providing an initiation mechanism, these lifting processes can also act to locally enhance convective available potential energy (CAPE) and reduce convective inhibition (CIN). Thus, understanding the mechanism by which a particular QSCS forms requires datasets with high spatial and temporal resolution. Investigations of these events have therefore typically relied on remotely sensed observations (from ground-based radar and satellites) and numerical simulations.

1
2
3 The existing body of work on QSCSs is dominated by
4 case studies of extreme flash flood-producing events in
5 the USA (e.g. Maddox *et al.* 1978; Petersen *et al.* 1999;
6 Schumacher and Johnson 2008) and the Mediterranean
7 region (e.g. Romero *et al.* 2000; Ducrocq *et al.* 2008;
8 Miglietta and Regano 2008). Comparatively few studies
9 have investigated these systems in the UK. One oft-cited
10 piece of work is that of Golding *et al.* (2005; hereinafter
11 GCM05), which examined the 'Boscastle storm' of 16
12 August 2004. This QSCS formed along and just inland
13 of the west coast of the UK Southwest Peninsula (Figure
14 1), and remained stationary for several hours, resulting in
15 rainfall totals which exceeded 200 mm over a narrow swath
16 of land (Burt 2005). The steep and rocky local catchments
17 rapidly channelled this water downstream, leading to
18 devastating flooding in the coastal settlements of Boscastle
19 and Crackington Haven (see Figure 1 for locations).

20
21
22
23
24
25
26
27
28
29
30 GCM05 investigated the Boscastle case using available
31 observations and numerical simulations with a high-
32 resolution ($\Delta x = 1$ km) version of the Met Office Unified
33 Model (UM). They found that deep convection was initiated
34 and maintained by a persistent, narrow convergence line
35 which developed along the coastline during the day. Based
36 on the results of sensitivity tests, the authors concluded
37 that this convergence line was 'a sea-breeze front whose
38 position was determined by a subtle balance between the
39 gradient wind direction, retardation and backing of the wind
40 over land, and differential heating'. They also suggested
41 that the modest instability in this case favoured 'closely
42 packed storms with weak downdraughts that did not distort
43 the coastal convergence line'. The intensity of the rainfall,
44 which was estimated to have exceeded 500 mm hr^{-1} for
45 brief periods (Burt 2005), appeared to be the result of
46 high tropospheric humidity, sustained by large-scale ascent,
47 which promoted unusually high precipitation efficiencies.

48
49
50
51
52
53
54
55
56
57
58
59
60 While the Boscastle storm was a rare and extreme
event, the development of persistent convergence lines
and associated convective showers over the UK Southwest
Peninsula is a relatively common occurrence. Monk (1987)

and Hand (2005) both noted the tendency for lines of
convective cloud, co-located with a well-defined zone of
near-surface convergence, to develop along and downwind
of the Southwest Peninsula in southwesterly flow. These
features occur most frequently during the Spring and
Summer from around midday to early evening (i.e.
when the land is warmer than the sea), suggesting that
sea breeze circulations play an important role in their
formation. However, other factors, such as differential
surface roughness may also be significant, as suggested by
GCM05.

In this paper, we present an analysis of a QSCS which
was remarkably similar to the Boscastle storm in terms of
its location and structure, though significantly less severe
in terms of its impact. The storm occurred on 21 July
2010 and produced around 50 mm of rain in 3 hours,
with no reports of flooding. This case provides an excellent
opportunity to investigate the factors which distinguish
a severe (i.e. flash flood-producing) QSCS from a non-
severe QSCS, without the complications associated with
comparing events in different geographical locations. It
also allows us to build on the work of GCM05 and Monk
(1987) by examining a range of factors (differential surface
heating, differential surface roughness, orography, and
convective outflow) which might influence the formation
and maintenance of convective lines in the Southwest
Peninsula. The latter objective is achieved through a series
of simulations using the operational UK Variable-resolution
(UKV) configuration of the UM. Although the horizontal
resolution of this model ($\Delta x = 1.5$ km over the UK) is
slightly coarser than that employed by GCM05, the two are
sufficiently similar to allow for a meaningful comparison of
results. The accuracy of the model simulations is assessed
through detailed comparisons with radar-derived surface
rainfall data. Furthermore, we investigate the impact of
increased horizontal resolution on forecast accuracy via a
simulation with 500-m grid spacing.

The rest of this paper is organised as follows. Section
2 describes the synoptic setting on 21 July 2010, the

1
2
3 evolution of the quasi-stationary storm, and the resulting
4 precipitation distribution. The differences between this
5 event and the Boscastle case are then discussed. Section 3
6 describes the UM and the UKV configuration, along with
7 the experimental design for our numerical investigation. In
8 Section 4, a control simulation is presented and compared
9 to observations. Results from a series of sensitivity
10 experiments are then used to demonstrate the mechanism
11 by which convective cells repeatedly developed in the same
12 location. Following this, results from the 500-m grid length
13 simulation are discussed. Finally, Section 5 presents a
14 summary and discussion of our findings.

2. Case study: 21 July 2010

15
16 We first examine the 21 July 2010 QSCS event in terms
17 the evolution of the large-scale flow, the life-cycle of
18 the convective system, and the resulting precipitation
19 distribution. We then compare each of these aspects with
20 the Boscastle storm of 16 August 2004.

2.1. Synoptic setting

21
22
23
24
25
26
27
28
29
30
31
32
33
34
35
36
37
38
39
40
41
42
43
44
45
46
47
48
49
50
51
52
53
54
55
56
57
58
59
60
The synoptic situation over the British Isles at 0600 UTC
(0700 British Summer Time, BST) on 21 July 2010 was
characterised by a slow-moving low-pressure system at
the surface and a cut-off low at upper-levels (Figure
2a). The centre of the surface low was located over the
northeast coast of England, while a secondary, weaker
circulation centre was present over southeast Ireland. The
Met Office surface analysis for this time (available online
at http://www.wetter3.de/Archiv/archiv_ukmet.html) shows
a cold front over the east coast of England, a warm front
running northeast from the main low centre to Norway,
and a trough line extending south from the secondary
circulation centre. Over the Southwest Peninsula, the
surface flow was from the southwest; i.e. roughly parallel
to the western coastline (Figure 2a). Quasi-geostrophic
forcing in the region was minimal, due to weak cold
air advection and cyclonic vorticity advection aloft (not
shown). Furthermore, the peninsula was not positioned

under any favourable regions for ascent associated with
upper-level jet streaks (not shown). As the day progressed,
the cyclone and associated cut-off low aloft moved very
slowly northeastward. This resulted in veering winds with
time over the Southwest Peninsula such that by 1800 UTC
(Figure 2b), the surface flow over the west coast was
approximately zonal.

The radiosonde ascent from Camborne, Cornwall (see
Figure 1 for location) at 1200 UTC on 21 July 2010 is shown
as a tephigram in Figure 3a. The atmosphere at this time
was characterised by an absolutely unstable surface layer,
moist, conditionally unstable air below a weak temperature
inversion at 700 hPa, and drier, absolutely stable air aloft.
In this situation we would expect surface-based convection
to readily develop, with strong updraughts in the lower
troposphere but rapid loss of buoyancy above 700 hPa.
We would also expect downdraughts to be relatively weak
due to the high humidity ($RH > 80\%$) below 700 hPa
which will have limited the potential for evaporation of
hydrometeors. Using an undilute pseudo-adiabatic parcel
ascent initialised with the average properties of the lowest
100 m, we find CAPE (calculated using virtual potential
temperature) of 122 J kg^{-1} and no CIN, with the lifting
condensation level (LCL) and LFC at 929 hPa (670 m), and
the level of neutral buoyancy (LNB) at 576 hPa (4.5 km).
However, surface-based parcels would be able to attain a
maximum altitude of around 450 hPa (6.3 km). The wind
profile in Figure 3a shows southwesterly flow over the depth
of the troposphere, with a density-weighted cloud layer–
mean wind speed of 11 m s^{-1} . The slight unidirectional
shear in the cloud layer may have reduced the potential for
downdraughts to suppress the convective updraughts.

2.2. Storm evolution and rainfall accumulations

In the moist, conditionally unstable flow over southwest
England, convection readily developed during the morning
of 21 July. High resolution visible images from Meteosat
Second Generation (not shown) reveal the development
of shallow cumuli over much of the Southwest Peninsula

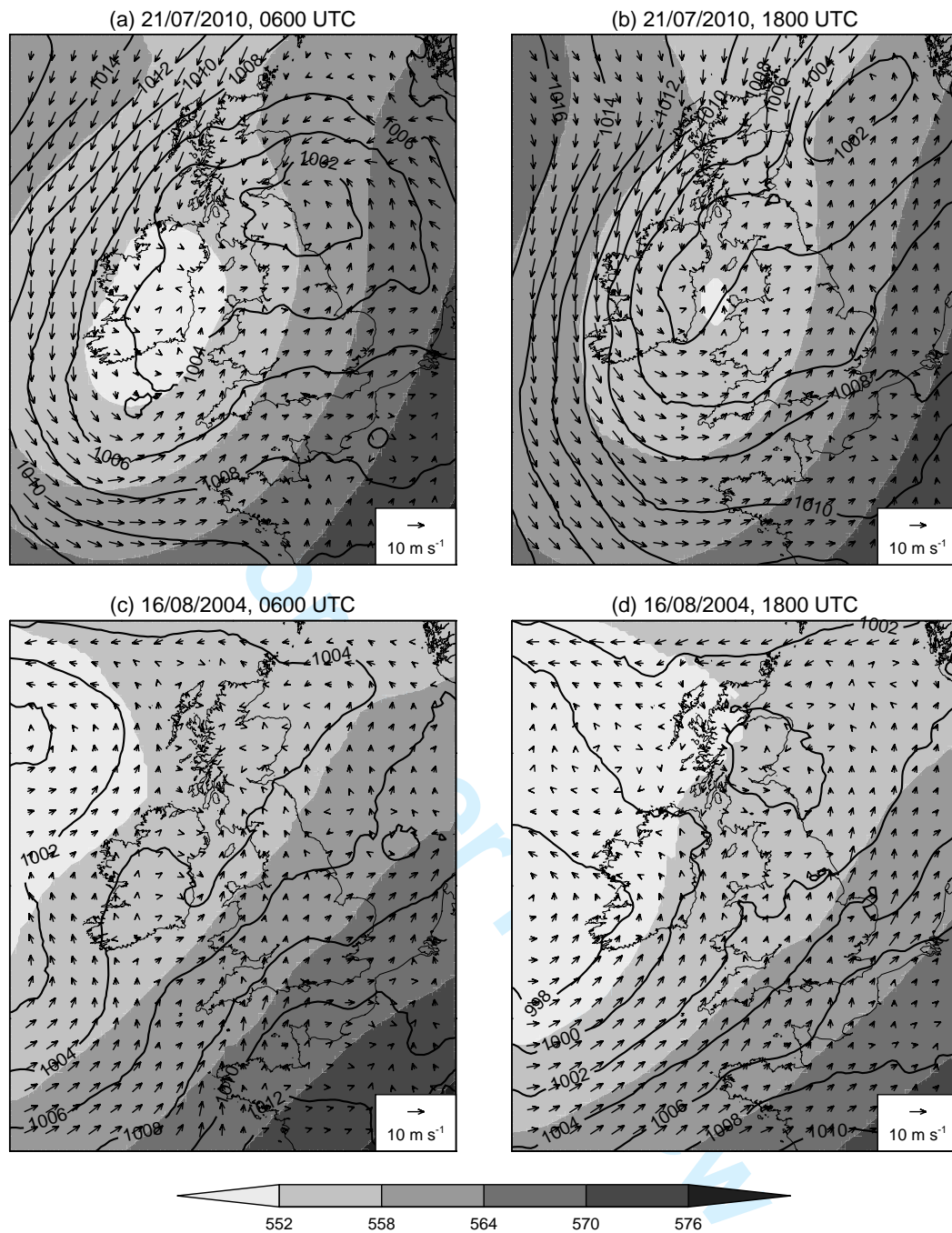


Figure 2. Unified Model 12-km grid length analyses for 0600 and 1800 UTC on 21 July 2010 (a, b) and 16 August 2004 (c, d) showing 500-hPa geopotential height (decametres, shading), mean sea-level pressure (hPa, contours) and 10-m wind vectors. Data for 21 July 2010 is from the operational North Atlantic and European (NAE) model of 2010; data for 16 August 2004 is from the operational Mesoscale Model of 2004.

between 0700 and 0800 UTC. These clouds rapidly deepened and organised into bands (cloud streets) parallel to the prevailing southwesterly flow. Rainfall radar imagery from the Met Office Nimrod System (Golding 1998) shows that between 0830 and 1000 UTC, numerous precipitating cells formed over the peninsula, in particular along and just inland of the west coast (Figure 4a). These cells tracked northeast at a speed of around 11 m s^{-1} , consistent with the

calculated cloud layer-mean wind. Over the next two hours, the cells increased in size and coverage, forming an almost continuous line of precipitation along the coastline (Figure 4b). The rainfall intensity also increased: around 1049 UTC, the tipping bucket rain gauge at Boscastle briefly recorded rain rates exceeding 150 mm hr^{-1} .

Following this, the line remained quasi-stationary for two hours, showing only slight inland movement between 1200

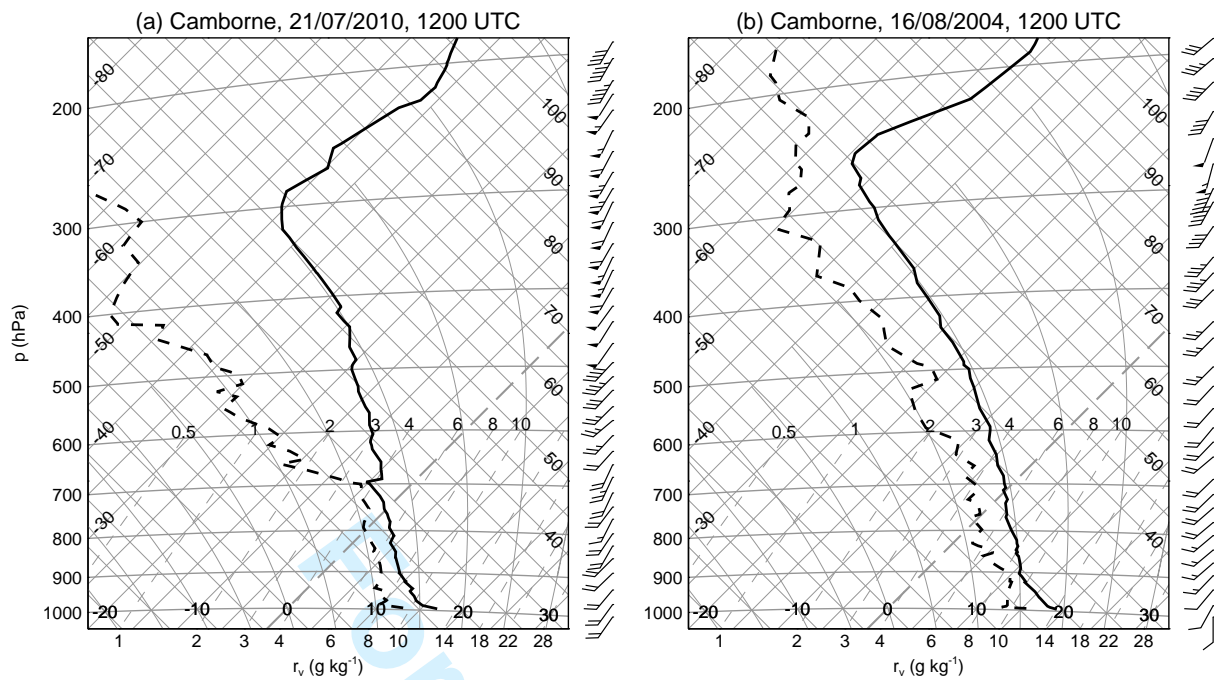


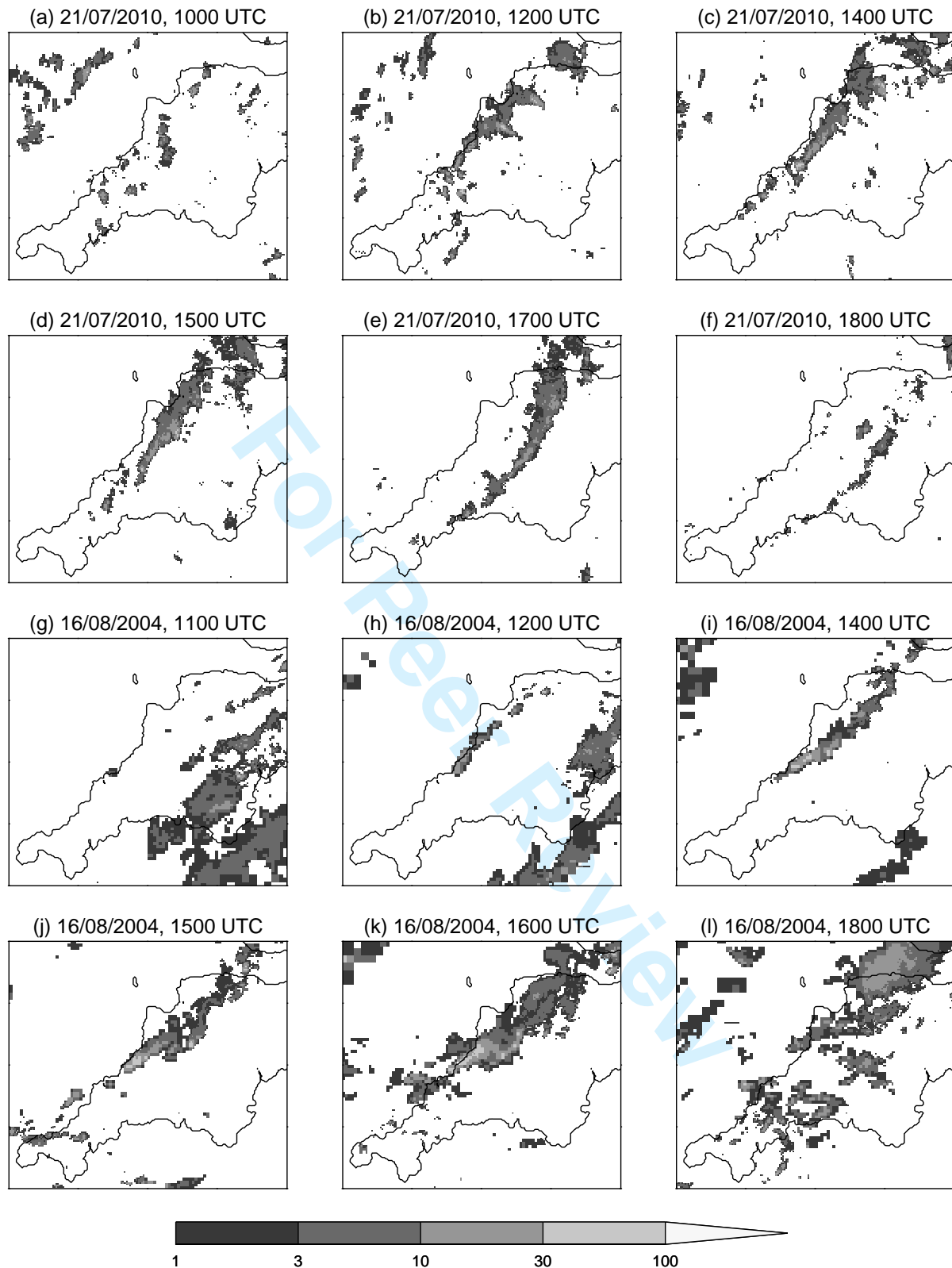
Figure 3. Tephigrams showing the 1200 UTC radiosonde ascents from Camborne on (a) 21 July 2010 and (b) 16 August 2004. Wind barbs show speed in knots with half barbs, full barbs, and pennants indicating 5, 10, and 50 knots respectively.

and 1300 UTC. At 1400 UTC (Figure 4c), the storm system was composed of two distinct areas. The first was the main convective line, with heavy precipitation extending from Bodmin Moor into Exmoor. The second, to the southwest of the first, consisted of slightly weaker, isolated cells located closer to the coastline. Animations of the rainfall field show that, in general, the southern cells did not merge with the main line but drifted to the west of it and dissipated. Meanwhile, the cells that made up the main line appear to have initiated farther east, along the centre-line of the peninsula. These cells rapidly intensified as they joined with the main line over Bodmin Moor, then continued northeast, weakening as they approached Exmoor and the Bristol Channel. Several of the more intense cells showed a sudden eastward progression as they approached the northeast end of the convective line (two such cells can be seen protruding from the main line in Figure 4b). This movement was likely related to the development and propagation of cold pools under the convective cells, with new initiation occurring along the gust front. Maximum cloud top heights (derived from Meteosat Second Generation imagery) were between

4.5 and 6 km at the northeast end of the line, consistent with the parcel analysis in Section 2.1.

After 1400 UTC, the convective line began to move inland, starting at its southwest end with the movement gradually spreading northeast (Figure 4d). The model simulations to be presented in Section 4 indicate that this movement was due to veering low-level winds associated with the gradual eastward progression of the surface cyclone (Figure 2). By 1700 UTC (Figure 4e), the line had moved away from the west coast, and extended in an arc from St. Austell Bay to Exmoor. Over the next hour, the system rapidly weakened (Figure 4f), eventually dissipating around 1900 UTC.

Figure 5a shows gauge and radar-derived rainfall accumulations between 1200 and 1500 UTC (i.e. the period for which the most intense portion of the line was stationary) over part of the Southwest Peninsula's west coast. Typical for a quasi-stationary storm, the precipitation area forms an elongated streak along the direction of cell motion, with sharp rainfall gradients either side (particularly, in this case, on the east side). Peak accumulations of around 50 mm occurred on the



55 **Figure 4.** Radar-derived surface rain rates (mm hr^{-1} ; $\Delta x = 1 \text{ km}$) over the Southwest Peninsula at various times on 21 July 2010 (a–f) and 16 August
56 2004 (g–l).

57
58
59
60
northwest slopes of Bodmin Moor; not an insignificant amount of rainfall for a 3-hour period, particularly over such fast-response catchments. However, there were no reports of flooding and the effect of the rain on river levels

was 'unremarkable' (Maggie Summerfield, Environment Agency, personal communication). There was a rapid rise in the level of the River Otter shortly after 1500 UTC noted at the Canworthy Water flood warning station (indicated with

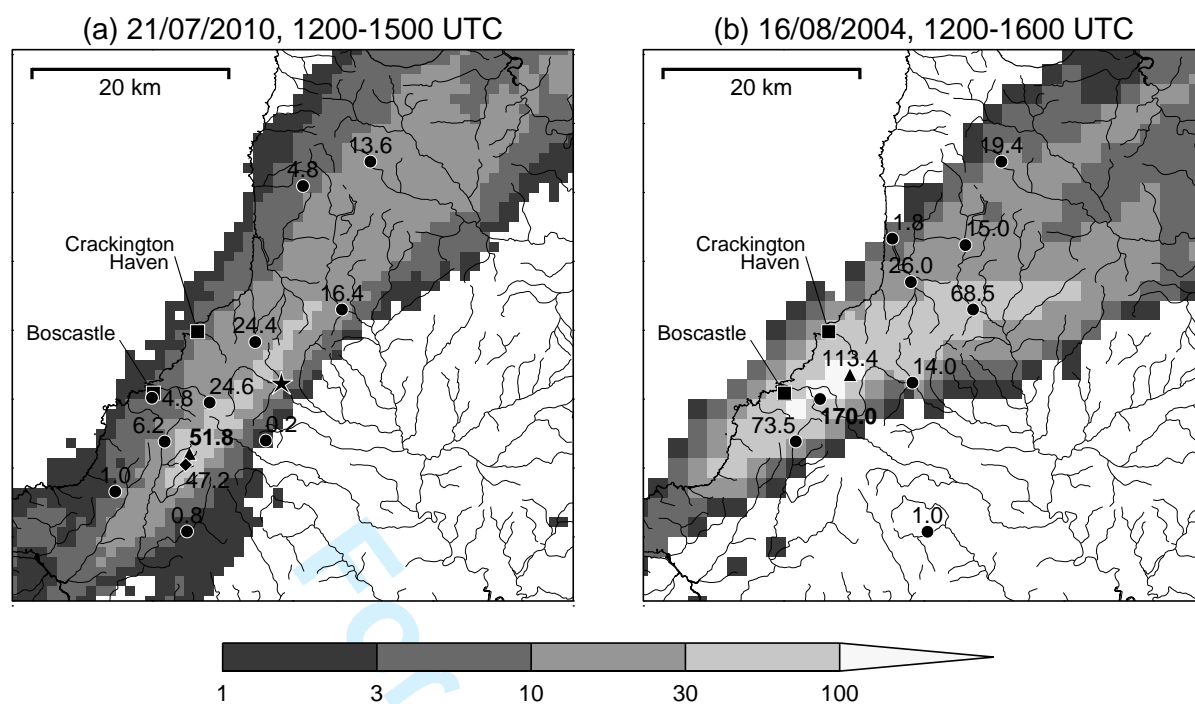


Figure 5. Radar-derived rainfall accumulations (mm, shading; $\Delta x = 1$ km) over a portion of the Southwest Peninsula for (a) 1200–1500 UTC on 21 July 2010 and (b) 1200–1600 UTC on 16 August 2004. Triangles indicate the maximum radar accumulation. Circles indicate accumulations from Environment Agency tipping-bucket rain gauges. The highest accumulation in each event is shown in bold. Note that the value for the Lesnewth gauge (maximum accumulation in (b)) was determined using the corrected data from Burt (2005). The diamond in (a) indicates the accumulation from the Met Office day (0900–0900 UTC) recording gauge at Lower Moor. The star in (a) shows the location of the Environment Agency’s Canworthy Water flood warning station. Thin contours show rivers from the Ordnance Survey GR dataset (<http://sharegeo.ac.uk/handle/10672/85>).

a star in Figure 5a), but the level attained happens many times a year. The lack of a significant hydrological response can be explained by the distribution of the heaviest rain across river catchments. Figure 5a reveals that the highest accumulations occurred close to the headwaters of several rivers, thereby spreading the runoff across multiple drainage basins. In contrast, in the Boscastle case, the heaviest rain fell to the west of the high ground, over just a handful of small coastal catchments (Figure 5b).

2.3. Comparison to Boscastle case

Figures 2–6 provide a comparison of the 21 July 2010 case and the Boscastle case, in terms of the large scale situation, the evolution of the convective systems, and the resulting precipitation. A detailed discussion of the Boscastle case is outside the scope of this paper, but can be found in Burt (2005), GCM05, and Golding (2005). Here, we focus on the main similarities and differences between the two cases.

On 16 August 2004, a slow-moving weakly baroclinic low pressure system was again affecting the UK, but in

this case, the system was positioned farther west, over the Eastern Atlantic (Figure 2c–d). As was the case on 21 July 2010, southwesterly flow was present over the depth of the free troposphere at 1200 UTC (Figure 3b), with weak unidirectional shear. However, the large-scale evolution on 16 August 2004 did not act to significantly turn the wind with time; thus, deep, southwesterly flow was maintained throughout the day. Furthermore, winds were slightly weaker than on 21 July 2010. The 1200 UTC Camborne ascent (Figure 3b) shows that in contrast to the 2010 case, very little conditional instability was present on this day. Instead, the temperature profile was approximately moist-neutral over almost the entire depth of the free troposphere. It was also up to 4 K warmer below 450 hPa than on 21 July 2010. Furthermore, high humidity was not constrained to below 700 hPa, but extended over the entire column ($50 < RH < 95$ % up to 400 hPa). GCM05 suggested that this deep moist layer was the result of large-scale ascent associated with an upper-level jet streak (not shown). Based on the observed thermodynamic environment, we would

1
2
3 expect convection to be characterised by weak updraughts
4 and downdraughts, high liquid water content, and high
5 precipitation efficiencies. Repeating the parcel analysis
6 from Section 2.1, we find no CIN, CAPE of 378 J kg^{-1} , an
7 LFC (and LCL) pressure of 929 hPa (760 m) and an LNB
8 pressure of 314 hPa (8.9 km). However, GCM05 noted that
9 some mature cells in the Boscastle convective line reached
10 the tropopause at around 250 hPa (10.5 km).

11
12
13
14
15
16 Figure 4 provides a comparison of the evolution of
17 the 21 July 2010 QSCS and the Boscastle QSCS. The
18 similarity in the location and structure of the two systems
19 is striking; however, there are several important differences.
20 First, in the Boscastle case, convection initiated later: the
21 first precipitating cells along the west coast of the Peninsula
22 did not appear until around 1100 UTC. This suggests that
23 initially CIN was too high and/or lifting was too weak for
24 parcels to reach their LFC. Second, the rain rates in the
25 convective cores of the Boscastle system were considerably
26 higher. Comparing Figures 3a and b, we note several
27 features of the environment which may have favoured more
28 intense precipitation on 16 August 2004:

- 29
30
31
32
33
34
35
36
37
38
39
40
41
42
43
44
45
46
47
48
49
50
51
52
53
54
55
56
57
58
59
60
- (i) Higher specific humidities throughout the troposphere. This indicates the presence of more water vapour available for condensation and precipitation formation (26 mm of precipitable water compared with 20 mm in the 2010 case).
 - (ii) Higher relative humidities at mid-levels. This will have reduced the detrimental effects of entrainment on cloud liquid water content (and buoyancy) favouring higher precipitation efficiencies.
 - (iii) Deeper warm and cold cloud layers (below and above the freezing level respectively). This may have simultaneously increased both warm-rain and ice-phase precipitation formation allowing for a more efficient collection of cloud droplets.
 - (iv) Weaker updraughts associated with a 'skinny' CAPE profile (small buoyancy excess throughout the cloud layer). This will have increased the in-cloud

residence time of rising air parcels, giving longer for precipitation growth (Davis 2001).

Despite moist sub-cloud layer air, the intense rain rates in the Boscastle case appear to have resulted in rapid downdraught formation, giving rise to bowing segments in the convective line to the northeast of Bodmin Moor (visible in Figure 4i, j, and k). The final important difference between the two cases was that the Boscastle storm remained stationary for a longer period of time. As previously noted, in the 2010 case the convective line began to move inland after 1400 UTC. In contrast, the Boscastle storm remained in place until 1630 UTC when it was swept northeast by a separate area of convection (visible southwest of the main line in Figure 4k). This difference appears to be related to the persistence of deep southwesterly flow in the Boscastle case, compared to veering flow in the 2010 case.

The result of these differences was a far more extreme rainfall event on 16 August 2004. While radar-derived totals for the Boscastle storm reached just over 110 mm between 1200 and 1600 UTC, corrected data from the Environment Agency's tipping-bucket rain gauge at Lesnewth (Burt 2005) shows an accumulation of 170 mm for this period (Figure 5b). This underestimation by the radar does not appear to have occurred on 21 July 2010: the total for the rainfall day (0900 UTC, 21 July–0900 UTC, 22 July) at the Met Office Lower Moor gauge (indicated by a diamond in Figure 5a) agrees well with the nearby radar maximum. Based on this fact, we present Figure 6 which compares rain rate and accumulation time series for the radar grid point with highest accumulation on 21 July 2010 with those for the Lesnewth gauge on 16 August 2004. This illustrates the relative impact of higher rain rates and longer rain duration in the Boscastle case. Extrapolation of the 2010 data suggests that had the storm persisted as long as the Boscastle QSCS, peak accumulations would have reached around 90 mm. This equates to roughly 30 % of the difference between the two events. Meanwhile, rain rates in the Boscastle case were around 30 mm hr^{-1} higher than

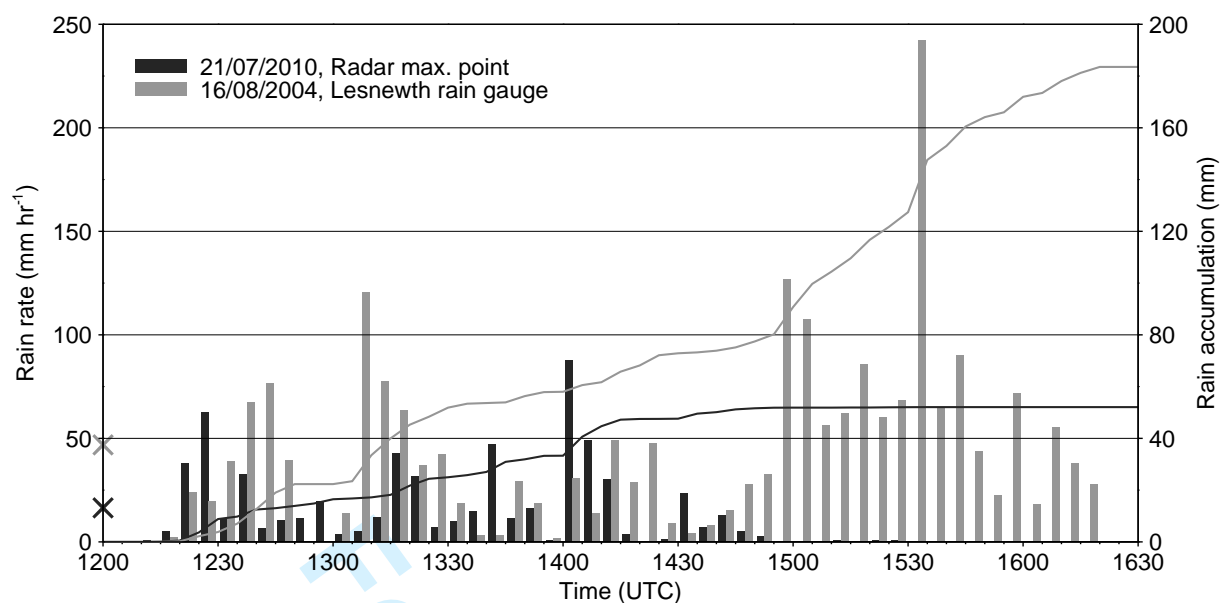


Figure 6. Time series of rain rate (bars) and rain accumulation (lines) for the point of maximum radar-derived rainfall accumulation on 21 July 2010 (dark grey) and for the Environment Agency's tipping bucket gauge at Lesnewth, Cornwall on 16 August 2004 (light grey). A heuristic correction has been applied to the Lesnewth data to account for under-reading during periods of intense rainfall (see Burt (2005) for details). Crosses on the y -axis show the average of rain rates ≥ 0.2 mm (the resolution of the tipping bucket gauge) for each case.

in the 2010 case (47 mm hr^{-1} compared to 16 mm hr^{-1}).

Of course, we can not know how intense the convective system on 21 July 2010 would have become had it remained stationary for longer. In the Boscastle case, the heaviest rain occurred after 1430 UTC, with over half the total (around 100 mm) falling in the 50 minutes from 1455 to 1545 UTC.

In summary, we note that while the 21 July 2010 QSCS showed clear similarities to the Boscastle QSCS of 16 August 2004, differences in the intensity, duration, and distribution of precipitation gave rise to very different impacts, with no recorded flooding in the former case and a devastating flash flood in the latter. However, the synoptic-scale conditions in both events were broadly similar, characterised by a slow-moving, weakly baroclinic low-pressure system to the west of the UK, with deep southwesterly flow and marginal instability over the Southwest Peninsula. In agreement with previous studies (Monk 1987; Hand 2005), this suggests that these conditions favour the development of QSCSs over the Southwest Peninsula. However, it is also clear that subtle differences in the characteristics and evolution of the large-scale flow can dramatically alter the severity of convective systems which develop.

3. Numerical model and experiment design

In order to investigate the mechanisms controlling the continued redevelopment of convection along the Southwest Peninsula west coast on 21 July 2010, a series of simulations were carried out using Version 7.3 of the Met Office Unified Model. This section describes the model and the design of the simulations.

3.1. The Unified Model

The Unified Model (UM) is a suite of numerical modelling software developed by the UK Met Office for simulating the atmosphere and other Earth-system components on a range of space and time scales. The UM solves the non-hydrostatic, deep atmosphere dynamic equations using a semi-implicit, semi-Lagrangian, predictor–corrector scheme (Davies *et al.* 2005). In the horizontal, the model uses a regular latitude–longitude grid with Arakawa-C staggering. For limited area configurations, the pole of the grid is rotated such that the domain is approximately centred on the equator, in order to minimise variations in grid length across the domain. In the vertical, the model uses a terrain-following, hybrid height coordinate with Charney–Philips staggering. The vertical grid spacing is smallest close to the

surface, in order to better resolve boundary layer processes, and decreases approximately quadratically with height. Parametrization schemes are used to represent a variety of sub-gridscale processes, including cloud condensation (Smith 1990), cloud and precipitation microphysics (Wilson and Ballard 1999), radiation (Edwards and Slingo 1996), surface exchange (Essery *et al.* 2003), boundary layer dynamics (Lock *et al.* 2000), and convection (Gregory and Rowntree 1990).

Among its many applications, the UM is the Met Office's operational numerical weather prediction (NWP) model and is used to produce global and regional deterministic and ensemble forecasts up to six days ahead. At Version 7.3, the deterministic nested suite consisted of four different configurations—Global, North Atlantic and European (NAE), UK 4-km (UK4), and UK Variable-resolution (UKV)—each producing four forecasts per day. The UKV model was used for the present investigation and is discussed further in the next section.

3.2. The UKV configuration

The UKV model is a limited-area, variable-resolution configuration of the UM. It was developed to improve the resolution of forecasts over the UK without the need for an intermediate-resolution model to properly treat boundary condition data from the 12-km grid length NAE model (Tang *et al.* 2012). The UKV horizontal domain consists of three sections: a coarse resolution ($\Delta x = 4$ km) outer frame, a fine resolution ($\Delta x = 1.5$ km) inner domain, and a variable-resolution transition area in-between (Figure 7). In the vertical, the model has 70 levels with a top at 40 km. At UM Version 7.3, the operational UKV was run at 0300, 0900, 1500 and 2100 UTC each day, with initial and boundary conditions provided by an NAE run initialised 3 hours earlier. A data assimilation cycle operated from $T - 2$ to $T + 1$ (where T is the forecast run time) which included assimilation of surface- and satellite-derived 3D cloud fractions (Renshaw and Francis 2011) and radar-derived surface rain rates (Jones and Macpherson 1997).

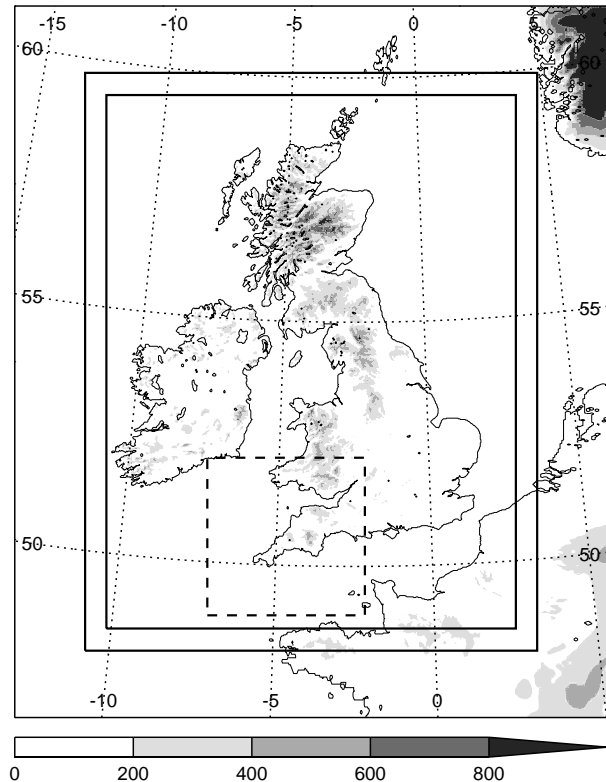


Figure 7. UKV model domain and orography height (metres). Inner and outer solid boxes show the limits of the constant resolution interior domain and the variable resolution transition zone respectively. Dashed box shows the domain used for our simulations. Dotted lines show true latitudes and longitudes.

A key feature of the UKV model is that it treats convection explicitly, i.e. without the use of a parametrization scheme. Since numerical models can only accurately represent processes larger than several grid lengths, individual convective cells (and in particular, their updraughts and downdraughts) are still significantly under-resolved with 1.5-km grid spacing. To truly capture the turbulent nature of DMC, one must apply large-eddy simulation (LES) techniques and use grid lengths of 100 m or less (Bryan *et al.* 2003). Despite this, $\mathcal{O}(1\text{-km})$ grid length configurations of the UM have been shown to provide substantial benefit in quantitative precipitation forecasting (QPF) for convective situations in the UK compared to lower-resolution configurations with parametrized convection (e.g. Roberts and Lean 2008; Lean *et al.* 2008).

3.3. Simulation strategy

Simulations of the 21 July 2010 QSCS have been carried out using the operational UKV configuration of the UM

at Version 7.3. Note that at the time of the event, the Met Office was actually running a slightly newer version (7.6); however, this was not available for the present investigation. All runs were initialised from the 0400 UTC operational UKV analysis (the output of the model's 3-hour data assimilation cycle) and integrated forward for 15 hours. As in the operational 0300 UTC run, lateral boundary condition (LBC) data were provided by the 0000 UTC NAE model forecast. A comparison of hourly surface rainfall fields from the operational forecast and our simulations (not shown) revealed generally good agreement.

In addition to a control simulation, a number of sensitivity tests were carried out in order to isolate the mechanisms responsible for the repeated initiation of convective cells along the peninsula coastline. These are discussed in detail in Section 4.2. A run with 500-m grid spacing was also performed and is described in Section 4.3. In order to minimise undesirable feedbacks on the large-scale flow in the sensitivity runs, and improve computational efficiency, all simulations were performed on a small domain nested within the full UKV model but with the same resolution ($\Delta x = 1.5$ km). This domain, shown by the dashed box in Figure 7, consists of 240×240 grid points which correspond exactly to points on the full UKV model grid (to eliminate the need for interpolation of the initial analysis). A single run of the full UKV model was used to provide LBCs for the nested domain at half hour intervals. The control run and all sensitivity tests were then run on the nested domain using the same initial and boundary condition data. Comparison between the output of the full UKV run and the control run (not shown) revealed some slight differences in storm evolution and precipitation accumulations; however, these do not affect the main findings of this investigation.

4. Simulation results

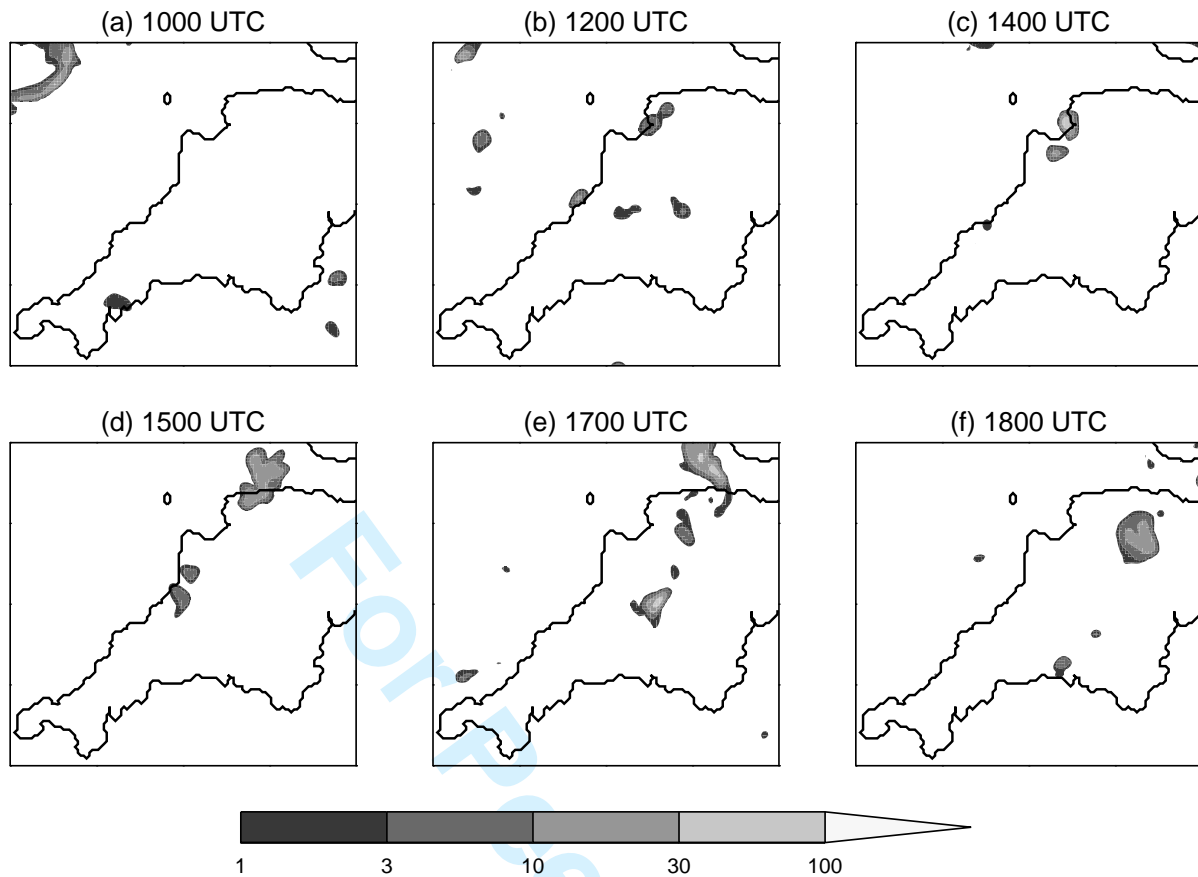
The following section presents results from the various simulations of the 21 July 2010 QSCS. Model data are presented on the rotated pole grid used in UK limited

area configurations of the UM. Where a direct comparison between model and radar data is required, the latter are bilinearly interpolated to the model grid.

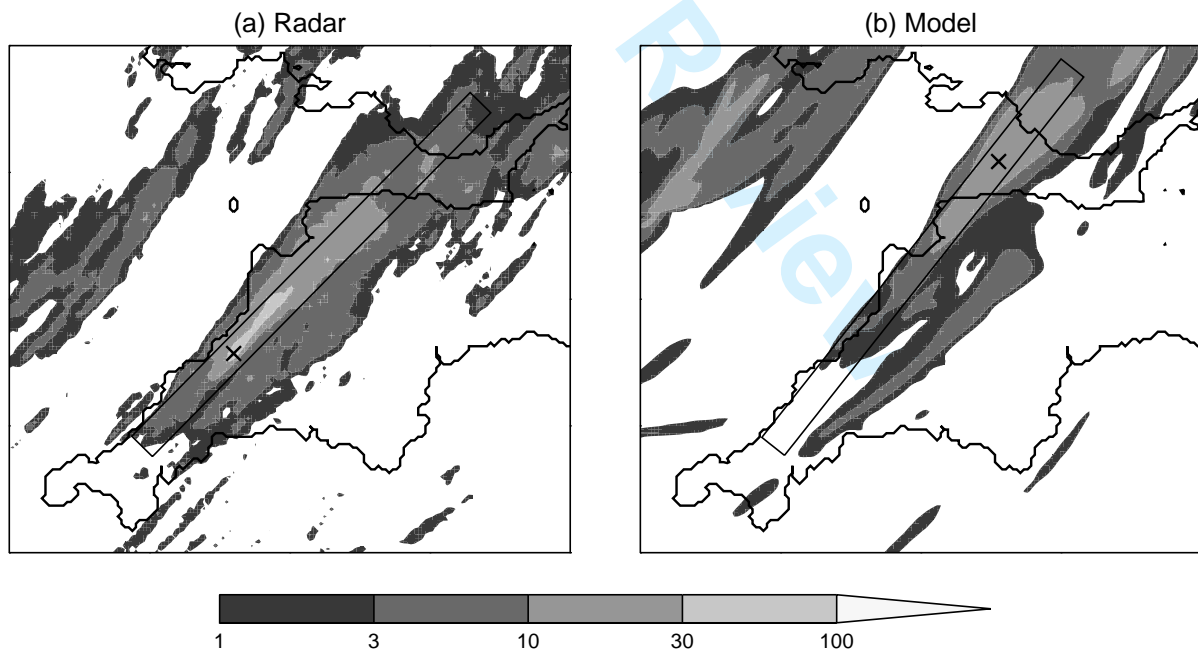
4.1. Control simulation

Figure 8 shows the evolution of the surface precipitation field in the control simulation. This can be directly compared with the observed evolution shown in Figure 4a–f. The model appears to have captured the repeated development of convective cells along the west coast of the peninsula during the late morning and early afternoon, and their subsequent inland propagation. However, there are some notable deficiencies in its representation of both the timing and structure of the storm system. These are further illustrated by Figures 9–11: Figure 9 compares the observed and simulated rainfall accumulations for 0900–1800 UTC; Figure 10 compares the observed and simulated rain intensity along the peninsula coastline for the same period using Hovmöller diagrams; Figure 11 shows histograms of the observed and simulated rain rates for the entire simulation period and domain.

First, the model initiates convection late, with the first precipitating cell appearing at 1000 UTC, over an hour later than in the radar data (Figure 10). The length of time (and thus the distance) between successive cells is also greater in the model. Consequently, the storm system fails to achieve the continuous, linear structure seen in the radar images. The cells themselves are smoother than those observed and too large, particularly during the mature stage of their evolution. Furthermore, they evolve too slowly in terms of the intensity of rainfall they produce (Figure 10). As noted in Section 2.2, the observed storms developed rapidly and produced heavy precipitation over Bodmin Moor where they joined the main convective line. As they approached the northeast end of the line in Devon, they generally weakened and became less organised (Figure 4a–f). By contrast, the modelled storms produce only light rainfall over Bodmin Moor and do not peak in intensity until they reach North Devon. Beyond this, they continue to grow



32 **Figure 8.** Evolution of surface rain rates (mm hr^{-1}) in the control simulation. The times shown match those for the radar images in Figure 4a–f.



56 **Figure 9.** Rainfall accumulations (mm) between 0900 and 1800 UTC on 21 July 2010 from (a) the radar and (b) the control simulation. Crosses mark the point of maximum accumulation. Boxes show the area for which Hovmöller diagrams (Figure 10) were calculated. These boxes both originate at the same point, are 200 km long and 10 km wide, and are orientated such that they pass through the points of maximum accumulation.

59 laterally and weaken only slightly as they move across the
60 Bristol Channel into Wales (Figure 8).

The net effect of these differences on the accumulated rainfall is shown in Figure 9. For the 9-hour period considered, the accumulation pattern associated with the

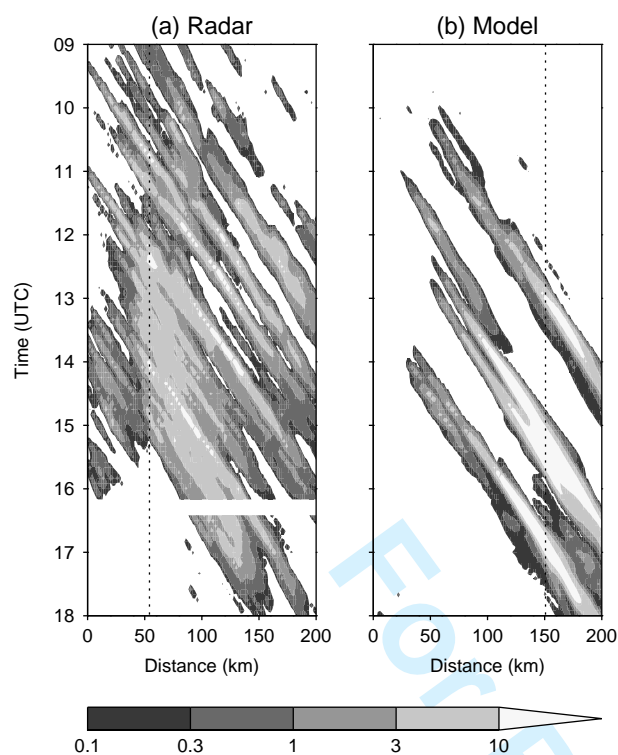


Figure 10. Hovmöller plots of rain rate (mm hr^{-1}) at 5-minute temporal resolution between 0900 and 1800 UTC on 21 July 2010 from (a) the radar and (b) the control simulation. These were computed along the boxes shown in Figure 9 with values averaged over the short axes (10-km width). Dotted lines show the locations of the maximum rainfall accumulation indicated in Figure 9. No radar data was available for 1615 and 1620 UTC. Note that the contour values in this figure are different from those in all other rain rate and rain accumulation plots.

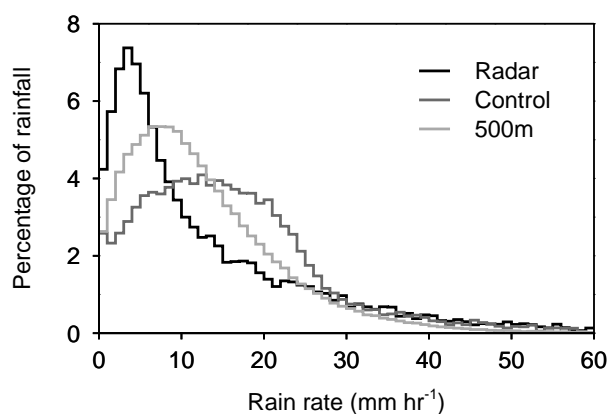


Figure 11. Histogram showing percentage contribution of rainfall rates (in 1 mm hr^{-1} bins up to 60 mm hr^{-1}) to grid points with rainfall accumulations $\geq 20 \text{ mm}$, computed over the entire control simulation domain and time period (0400–1900 UTC). Data are shown for the radar (black), control simulation (dark grey), and 500-m grid length simulation (light grey). Before processing, the radar data was interpolated to the model grid and the 500-m data was smoothed to the control simulation resolution using a 3×3 boxcar average at each grid point.

QSCS is fairly well captured; however, the maximum is less by a factor of two (25 mm compared to 50 mm) and shifted around 100 km to the northeast (Figure 10). This shift is primarily due to the slower development of cells in the model, which also results in reduced along-line

accumulation gradients on the upstream (southwest) side of the precipitation maximum. We might expect the difference in maximum accumulation to be greater given the wide spacing between successive cells in the model; however, this appears to have been at least partly compensated for by overly intense precipitation in the convective cores (Figure 10). Indeed, Figure 11 reveals that the simulation has a substantial positive bias in rain rates when compared to the radar observations. This is most pronounced when we consider only those grid points with high accumulations ($\geq 20 \text{ mm}$ in Figure 11) since these typically will have received the most intense rainfall.

Clearly there are some significant deficiencies in the representation of the 21 July 2010 QSCS in our control simulation. Some of these may be due to inadequate horizontal resolution, a possibility which is explored in Section 4.3 using a 500-m grid length simulation. However, a comprehensive investigation of all model biases is outside the scope of this work. Much research is ongoing into the ability of high-resolution configurations of the UM (and other operational models) to accurately forecast convective precipitation. Here, we note that while the simulation is far from perfect, it successfully captures the key process for QSCS development: the repeated generation of convective cells in roughly the same location. We therefore turn our attention to the initiation mechanism.

Based on the findings of GCM05 and Monk (1987), we would anticipate that lifting along a boundary layer convergence line was responsible for the repeated initiation of convection in the present case. An examination of the 10-m horizontal divergence field from the control simulation (Figure 12) confirms this to be the case. Over the course of the morning, areas of strong convergence (divergence $< -0.001 \text{ s}^{-1}$) develop along portions of the western coastline (Figure 12a, b). These gradually expand and join up, forming a quasi-continuous line by the early afternoon (Figure 12c) which subsequently moves inland (Figure 12d). The inland movement of the line after 1400 UTC appears to be due to a gradual veering of the

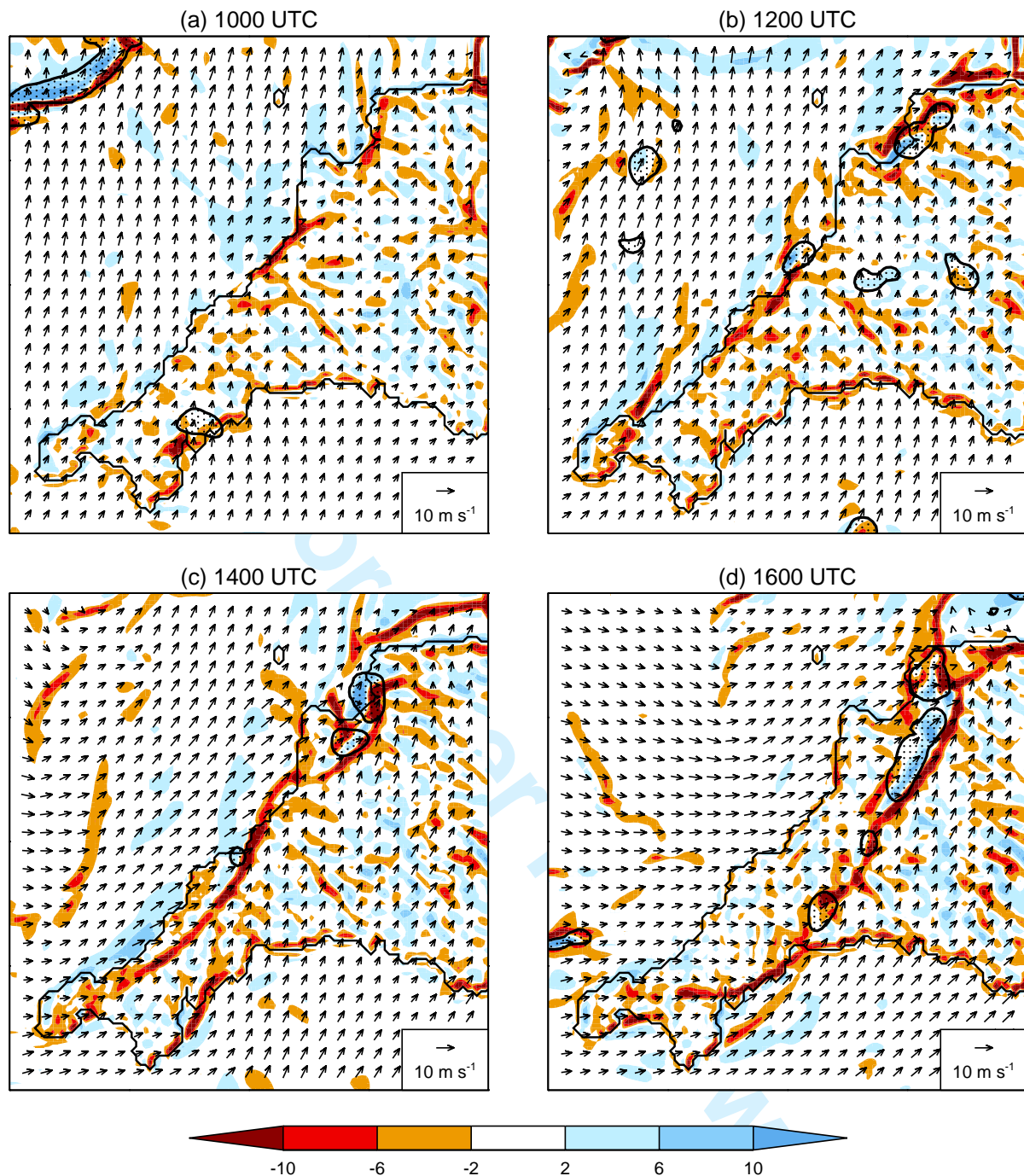


Figure 12. Wind vectors and divergence (10^{-4} s^{-1} , shading) at 10 m and surface rain rate greater than 1 mm hr^{-1} (black contours, stippled) in the control simulation at (a) 1000, (b) 1200, (c) 1400, and (d) 1600 UTC.

background flow associated with the eastward progression of the surface low-pressure system. Figure 12 shows that convective cells repeatedly develop and track along the northwest side of the convergence line and remain bound to it as it moves inland. Vertical cross-sections taken across the coastline (not shown) reveal that the low-level convergence is associated with an overturning circulation, approximately 1 km in depth, superimposed on the background wind

field, with vertical velocities up to around 1 m s^{-1} . At particular times and points along the line, this lifting was clearly sufficient for parcels to reach their LFC, initiating deep convection. The resulting cells were then advected northeast, parallel to the convergence line, which continued to supply them with moist, potentially buoyant air.

Figure 12 shows that the convergence line is associated with a change in wind direction from

southerly/south-southwesterly on the southeast (land) side to southwesterly/west-southwesterly on the northwest (sea) side. One might speculate that this results from frictional backing of the flow over land; however, in some locations the wind just offshore clearly veers towards the land. This veering is particularly pronounced at 1400 UTC (Figure 12c) at the southwest end of the coastline where it creates a stream of divergent flow emanating from the northern tip of the Land's End Peninsula (a feature that was also present in the Boscastle simulations of GCM05; their Figure 12). These observations are consistent with the idea of the convergence line as a sea breeze front: higher temperatures over land result in a pressure gradient directed from sea to land which in turn produces an onshore flow component (see Miller *et al.* (2003) for a review of the sea breeze system). To verify this hypothesis and determine the relative importance of the land–sea temperature contrast and frictional effects (as well as other potential influences), a series of sensitivity tests were performed. These are the subject of the next section.

4.2. Sensitivity tests

To investigate the origins of the simulated convergence line, we consider four factors which are known to generate and modulate regions of boundary layer convergence: differential surface heating, differential surface roughness, orography, and convective outflow. For the Boscastle case, GCM05 found that a positive land–sea temperature difference was critical to the formation of the convergence line, suggesting that it was a sea breeze front. Orography, meanwhile, was shown to slightly modulate the precise location of the line and the resulting distribution of precipitation. The authors also suggested the importance of frictional backing of the flow over land in creating an offshore flow component which balanced the sea breeze, maintaining the convergence line in place, and storm-generated outflow in distorting the convergence line at its northeast end. However, these factors were never formally addressed through sensitivity tests. Leoncini *et al.* (2012)

also performed simulations of the Boscastle case using a 1-km grid length version of the UM, including a run without the land–sea roughness contrast. In contrast to GCM05, the authors concluded that this was only a modulating factor in the formation of the convergence line.

Table 1 details how each of the sensitivity tests in the present investigation was carried out. Note that the methodology employed to remove the land–sea temperature contrast (the WEAKSUN run) is different from that in GCM05. Specifically, GCM05 fixed the land surface temperature and fluxes to values typical of nearby sea points, whereas we have simply reduced the solar constant. Our approach reduces insolation of the land surface, in turn reducing surface fluxes and thus boundary layer air temperatures. Sea surface temperatures, on the other hand, are fixed to climatological values, so fluxes and temperatures over sea points are not directly affected. As will be shown, the result is that the low-level land–sea air temperature difference remains negative throughout the simulation. While our approach is less direct than that of GCM05, it had the advantage of being very simple to implement in the model.

Figure 13 shows the impact of each sensitivity test on the low-level wind and divergence fields at 1400 UTC (c.f. Figure 12c). Surface precipitation is also shown; however, it is important to note that slight changes in the instantaneous position and size of the convective cells cannot be considered indicative of a systematic response to a particular change in model setup. The WEAKSUN run immediately stands out in Figure 13 due to the complete disappearance of the coastal convergence line. Consistent with this, the region of divergent flow emanating from the Land's End Peninsula is no longer present and the winds along much of the coastline have a reduced westerly component. This confirms the hypothesis that the veering flow offshore is a response to differential heating of the land and sea; i.e. it is part of a sea breeze circulation.

In contrast, the impact of the other sensitivity tests is relatively minor. As one would expect, reducing the

Table 1. Details of the sensitivity tests performed.

Name	Factor under investigation	Methodology
WEAKSUN	Differential surface heating	Solar constant reduced to 400 W m^{-2}
SAMEROUGH	Differential surface roughness	Roughness length for momentum over land and sea fixed to $4 \times 10^{-5} \text{ m}$
NOOROG	Orography	Land height over Southwest Peninsula set to 1 m
NOOUTFLOW	Convective outflow	Latent cooling due to rain evaporation and snow melt switched off

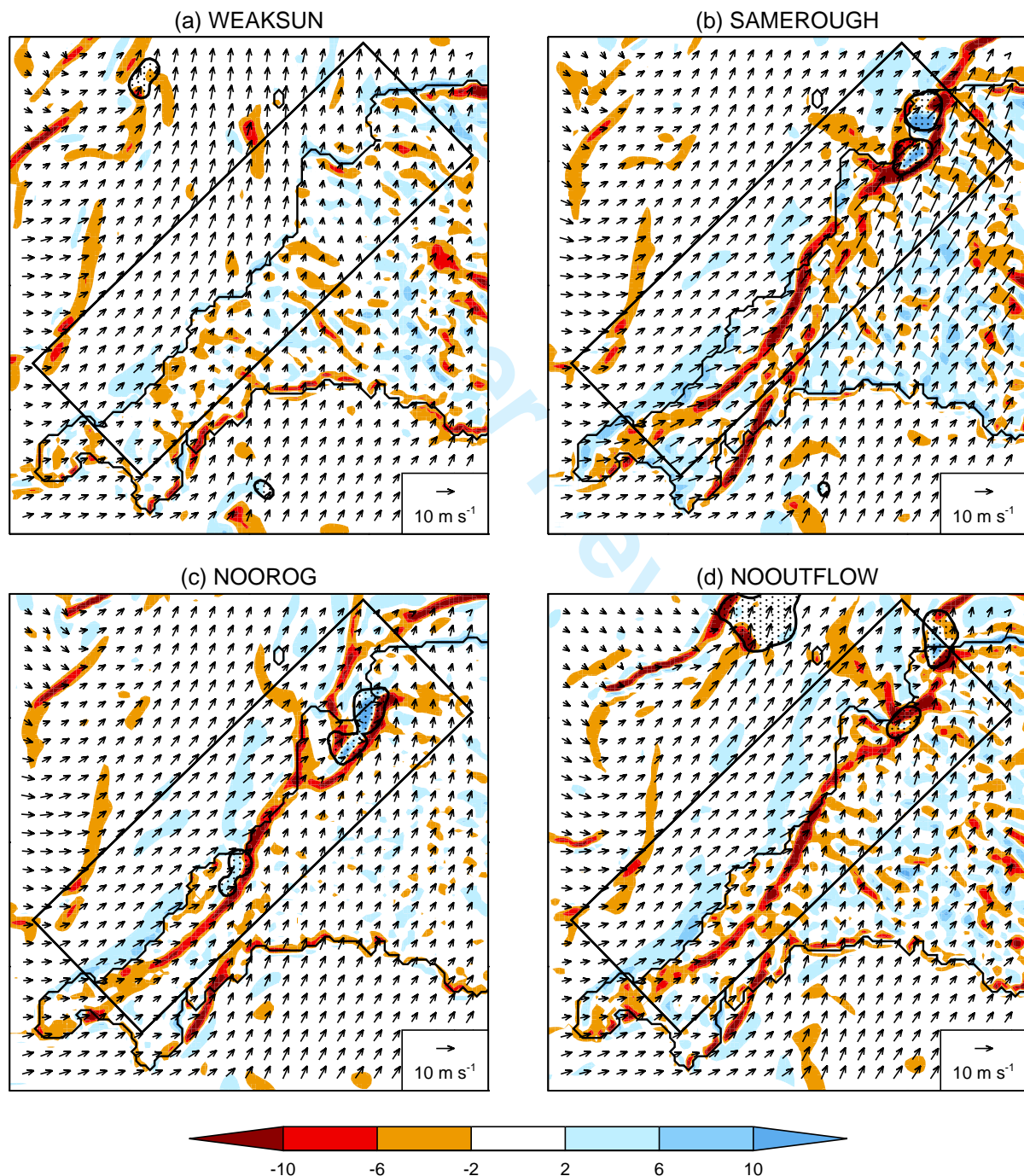


Figure 13. As in Figure 12 but for each of the sensitivity runs at 1400 UTC: (a) WEAKSUN, (b) SAMEROUGH, (c) NOOROG, and (d) NOOUTFLOW. Black boxes show the area for which the time series in Figures 14 and 15 were calculated.

land roughness (Figure 13b) results in higher wind speeds and veering (or rather, reduced frictional backing) of the flow. These two changes have counteracting effects on the convergence line: faster winds enhance convergence with the onshore flow along west coast, while clockwise turning of the wind reduces it. The net effect appears to be small. Thus, contrary to the conclusions of GCM05 but in agreement with Leoncini *et al.* (2012), frictional effects over land are not necessary for the development of this type of quasi-stationary convergence line.

Consistent with the findings of GCM05 (and Leoncini *et al.* 2012), flattening the orography also has a minor influence on the convergence line, though it does of course reduce small scale variations in the divergence field over land (Figure 13c). In the control simulation, convective outflow is apparent as localised areas of strong divergence coinciding with precipitating cells (Figure 12). These are clearly absent in the NOOUTFLOW run (Figure 13d), but this again has little overall impact on the convergence line.

Animations of the divergence field for the control run reveal that convective outflow may have locally enhanced and distorted the convergence line; however, it was too weak to substantially influence the evolution of the line or the associated convection. As noted in Section 2.2, in reality, several cells at the northeast end of the line showed a sudden eastward movement, presumably associated with propagating cold pools. The failure of the control simulation to capture this occurrence perhaps relates to the wide spacing between convective cells. This will have allowed outflow to spread out in both the along-line and cross-line directions, whereas in reality, adjacent cold pools may have merged, restricting motion to only the cross-line direction.

Figure 14 summarises the evolution of each simulation in terms of a number of key variables: mean land–sea temperature difference at 1.5 m, mean 10-m zonal wind over the sea, number of grid points with ‘strong’ 10-m wind convergence (divergence $\leq -5 \times 10^{-4}$), and mean surface rain rate. To focus attention on the area of interest, each of these has been computed over the box shown in

Figure 13. As we would expect, the land–sea temperature difference (Figure 14a) follows the diurnal cycle of surface heating over land, increasing during the morning and early afternoon, peaking around 1400 UTC, and then decreasing again thereafter. However, in the WEAKSUN run, values remain negative throughout the day. Some localised areas of positive land–sea temperature difference do occur (not shown), but on average the low-level air over this part of the Southwest Peninsula remains cooler than that over the sea. Note that the higher temperatures in the NOOROG run are purely a result of the lower land elevation. The low-level zonal wind over the sea (Figure 14b) increases throughout the day, partly in response to the evolution of the large-scale flow (Section 2.1), but also due to veering associated with the land–sea temperature difference. The absence of the latter effect in the WEAKSUN run is evident, with a reduced westerly component during most of the day.

Regions of strong convergence exist at the start of the simulations (Figure 14c) due to land breezes, with cool air descending down the hills of the peninsula and moving out across the sea. The land breezes decay during the subsequent hours as insolation warms the land, reversing the thermal pressure-gradient acceleration; however, this process is retarded in the WEAKSUN run. In the other simulations, regions of strong convergence again start to form after 0830 UTC, associated with the development of the sea breeze circulation. These are slightly stronger in the SAMEROUGH simulation due to faster winds over land. Convergence peaks between 1330 and 1500 UTC, coincident with the development of heavy precipitation (Figure 14d), and decays thereafter as the line moves inland and out of the box. In contrast, in the WEAKSUN run, convergence remains weak, increasing only slightly between 1400 and 1600 UTC with the passage of a transient feature associated with the base of the surface pressure trough (Figure 14c). Consequently, no heavy convective precipitation develops in this simulation (Figure 14d).

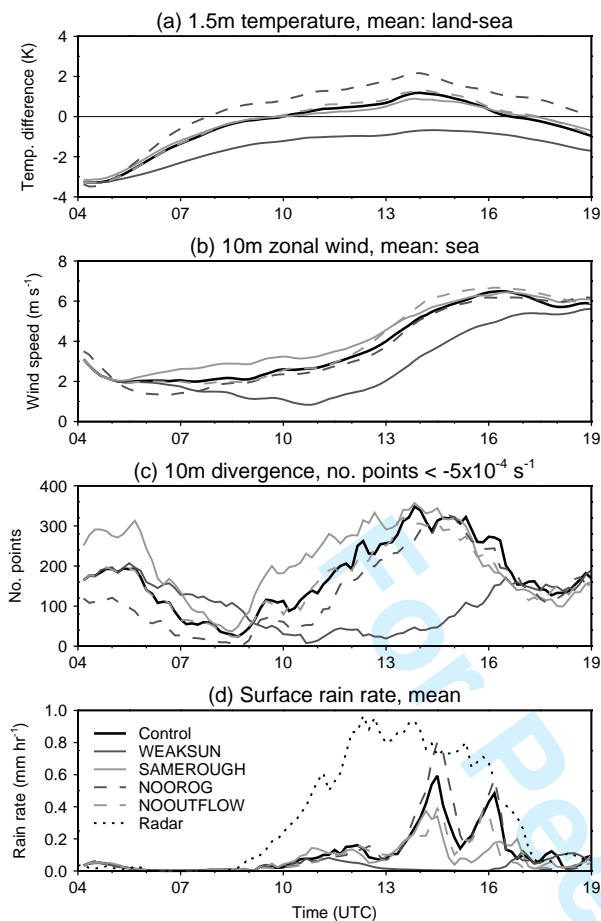


Figure 14. Time series of four quantities from the control simulation (black, solid) and each of the sensitivity runs—WEAKSUN (dark grey, solid), SAMEROUGH (light grey, solid), NOOROG (dark grey, dashed), NOOUTFLOW (light grey, dashed)—computed over the box shown in Figure 13: (a) difference between mean 1.5-m temperatures over land and sea points; (b) mean 10-m zonal wind component over sea points; (c) number of points with 10-m wind divergence less than $-5 \times 10^{-4} \text{ s}^{-1}$; (d) mean surface rain rate. Rain rates from the radar (black, dotted) are also shown in (d). Data are plotted with a time resolution of 10 minutes.

4.3. 500-m grid length simulation

In Section 4.1, it was noted that the control simulation shows a number of deficiencies in its representation of the 21 July 2010 QSCS. These include late initiation of convection, cells that are too large, intense, and widely spaced, and slow convective evolution. It has also been noted that with 1.5-km grid spacing, convective storms are still significantly under-resolved. One might therefore anticipate that increasing the resolution would improve the model's representation of this event. To test this hypothesis, a simulation with a grid length of 500 m was performed using an existing experimental configuration of the UM. The same domain, nested within the full UKV model, was used in this simulation but with triple the

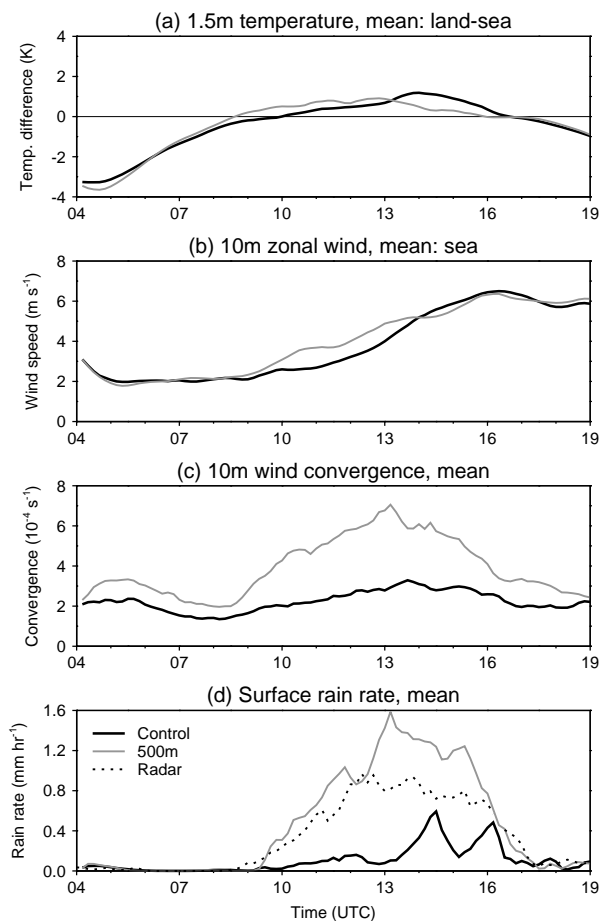


Figure 15. Similar to Figure 14, but comparing the control simulation (black, solid) and the 500-m grid length simulation (grey, solid). In this Figure, (c) shows the mean convergence; i.e. the mean of all points with divergence < 0 .

horizontal resolution (718×718 grid points). The vertical grid was not altered. Orography and other ancillary data were initially kept at the same resolution and bilinearly interpolated to the 500-m grid. However, it was found that this simple interpolation method concentrated the curvature of the orography field at the original (UKV model) grid points, creating spurious regions of low-level convergence and divergence. To alleviate this problem, the interpolated orography data was smoothed using a 3×3 boxcar moving average. As in previous simulations, the 0400 UTC operational UKV analysis was used as initial conditions, LBCs were provided by the full UKV run, and the model was integrated forward for 15 hours.

Figure 15 compares the evolution of the 500-m run to that of the 1.5-km control run in an almost identical manner to Figure 14, the only difference being that Figure 15c shows mean convergence rather than the number of 'strong'

1
2
3 convergence points. This change is necessary due to the
4 greater number of grid points and the overall increase in
5 convergence discussed below. The impact of the resolution
6 change on the land–sea temperature difference (Figure 15a)
7 and zonal wind over sea points (Figure 15b) is relatively
8 small. Both are slightly enhanced during the late morning
9 and early afternoon in the 500-m run. This appears to be
10 the result of reduced cloud cover, which leads to enhanced
11 shortwave heating of the land surface and a slightly
12 stronger sea breeze circulation. Far more dramatic changes,
13 however, are seen in the convergence and precipitation
14 fields. Throughout the simulation, but especially from
15 0900–1600 UTC, convergence is enhanced in the 500-m
16 run (Figure 15c). The rapid increase in convergence around
17 0900 UTC is shortly followed by the development of heavy
18 precipitation (Figure 15d). When compared to the radar
19 observations, the 500-m run shows vast improvements in
20 the timing and rate of convective development, although it
21 overdoes the area-averaged rainfall intensity.

22
23
24
25
26
27
28
29
30
31
32
33
34 To better illustrate the changes in precipitation, wind, and
35 divergence, we present Figure 16, which shows a snapshot
36 of these fields at 1400 UTC in the 500-m run. Comparison
37 of Figure 16a with Figure 4c (observed rainfall) and Figure
38 8c (control simulation rainfall), shows that increasing
39 the horizontal resolution has somewhat improved the
40 model's representation of the structure of the storm system:
41 cells are more numerous, more closely packed, and have
42 enhanced fine-scale structure. Animations reveal that the
43 storm evolution, including the eastward propagation and
44 weakening of cells at the north end of the line, is also
45 more in line with observations. Furthermore, Figure 11
46 demonstrates that the positive bias in rain intensity, while
47 still present, is significantly reduced in the 500-m run.
48 Despite these improvements, the representation remains
49 far from perfect. This may be because the convective
50 overturning process is still under-resolved (Bryan *et al.*
51 2003), but there are many other potential sources of error.
52 In particular, most of the UM's parametrization schemes
53 were designed to produce optimal forecasts at much coarser

resolutions—the best settings for very high resolutions
($\Delta x < 1$ km) are still being actively investigated.

Turning to the divergence field (Figure 16b; c.f. Figure
12c), the most striking change is in the scale and magnitude
of the maxima and minima. Most significantly for this
case, the convergence line is stronger and narrower with
values up to and exceeding $-5 \times 10^{-3} \text{ s}^{-1}$ over a width of
just 3–5 grid points. The wind field meanwhile is changed
very little. This shows that as we increase the resolution,
the horizontal scale over which the wind varies decreases
accordingly, allowing for enhanced convergence/divergence
and associated vertical motions. Cross-sections (not shown)
confirm the presence of stronger low-level ascent and
an associated deepening of the boundary layer along
the convergence line. For the present case, this change
is significant in determining the timing and pattern of
convective initiation.

5. Summary and discussion

We have presented an analysis of a quasi-stationary
convective system which formed over the UK Southwest
Peninsula on 21 July 2010. This system showed remarkable
similarity to the flash flood-producing Boscastle storm
of 16 August 2004. In both events, convective cells
repeatedly developed and moved along and just inland of
the peninsula's west coast, producing intense precipitation
over a narrow swath of land. However, maximum rainfall
accumulations were approximately four times smaller in the
2010 case and no flooding was recorded. This difference
is related to three factors: the intensity of the rainfall,
the duration of convective systems, and the distribution
of the rainfall across drainage basins. In the Boscastle
case average rainfall rates were around three times higher
than those in the 2010 case. This was likely related to
several characteristics of the environment, including greater
precipitable water, higher mid-level relative humidities,
greater cloud depth both above and below the freezing
level, and weaker updraughts. The Boscastle storm also
remained quasi-stationary for around 90 minutes longer

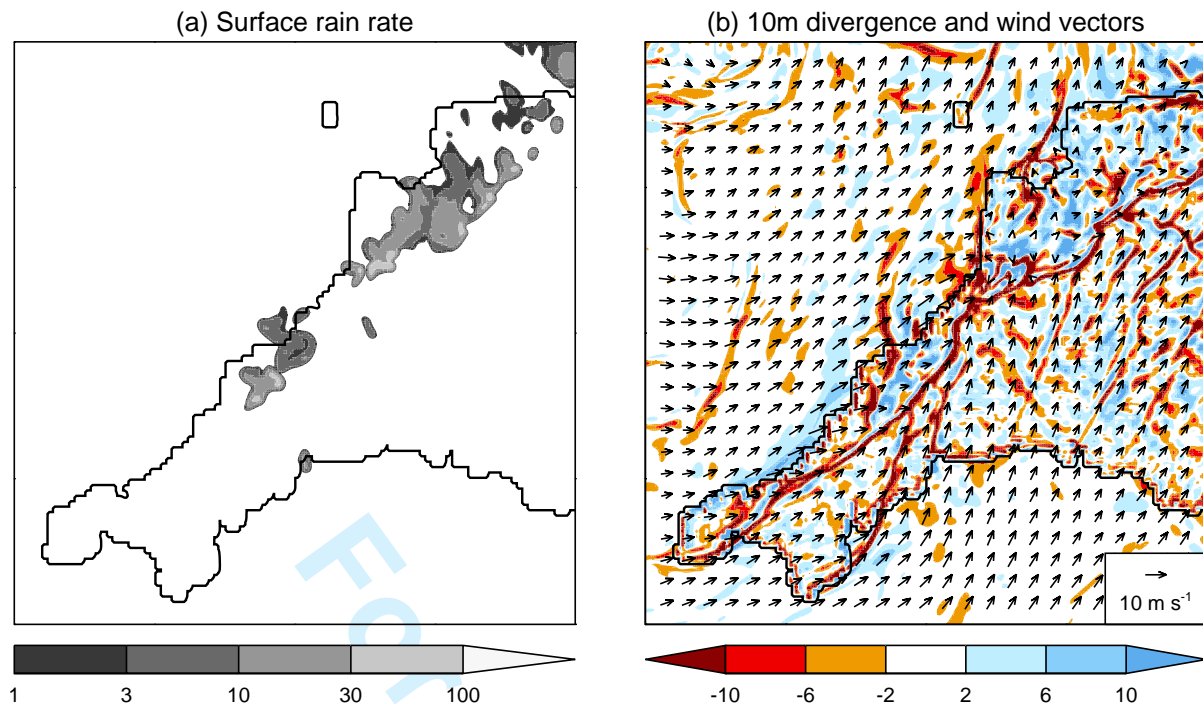


Figure 16. Output from the 500-m simulation at 1400 UTC: (a) Surface rain rate (mm hr^{-1}); (b) 10-m wind vectors and divergence (10^{-4} s^{-1}).

than the 2010 storm due to slower evolution of the wind field: in the latter case, veering low-level flow caused the convective system to move inland several hours before it dissipated. Finally, slight differences in the location of the two storms meant that in the Boscastle case, the heaviest rainfall was distributed over fewer river catchments, further enhancing the hydrological response. Overall, however, large-scale conditions in both events were broadly similar, characterised by a slow-moving, weakly baroclinic cyclone to the west of the UK, with a marginally unstable air mass and unidirectionally sheared southwesterly flow over the Southwest Peninsula.

Numerical simulations of the 21 July 2010 event were performed using a 1.5-km grid length configuration of the Met Office Unified Model. A control simulation successfully captured the repeated development of convective cells along the coastline, but failed to accurately represent the narrow, linear structure of the storm system. The model also showed a substantial positive bias in instantaneous rain rates and underestimated the storm-total precipitation due to wide spacing between successive convective cells. Despite these biases, the simulation was suitable for investigating the

mechanism by which the QSCS formed. As in the Boscastle case, convective initiation was maintained by lifting along a quasi-stationary boundary layer convergence line. Sensitivity tests were performed to determine the mechanisms controlling this feature. In agreement with the findings of GCM05 for the Boscastle case, the convergence line was shown to be the result of a balance between the background flow over land and the near-surface component of a sea breeze circulation along the west coast. However, in contrast to a hypothesis put forward by GCM05, frictional turning of the wind over land was not found to be necessary for this process to occur. Furthermore, the effects of latent cooling-produced storm outflow and the orography of the Southwest Peninsula were not significant in the 2010 case.

To investigate the impact of enhanced horizontal resolution on the modelled storm system, a simulation with 500-m grid spacing was performed. This showed marked improvements in the timing of convective initiation, the structure of the convective system, and the rainfall intensity. Critical to the improvements in convective initiation was an increase in the strength of the convergence line, which allowed low-level air parcels to more readily reach

1
2
3 their LFC. This change can be attributed directly to an
4 improved representation of sharp horizontal wind gradients.
5
6 Observations of boundary layer convergence lines (e.g.
7 Wilson and Schreiber 1986; Wilson *et al.* 1992) reveal that,
8 in reality, the width of these features ranges from around
9 0.5 to 5 km. It is therefore not surprising that the 1.5-km
10 model failed to adequately resolve the convergence line,
11 particularly when we consider the additional smoothing
12 generated by numerical diffusion and the subgrid mixing
13 parametrization.
14
15
16
17
18

19
20
21 This final finding is important as it suggests that
22 in situations where boundary layer convergence is
23 the dominant mechanism of convective initiation, the
24 highest resolutions currently used operationally may still
25 be insufficient for quantitative precipitation forecasting.
26
27 Barthlott *et al.* (2010) reached a similar conclusion based
28 on simulations of a convergence line–forced thunderstorm
29 observed during the Convective and Orographically induced
30 Precipitation Study (COPS; Wulfmeyer *et al.* 2008).
31 They used the German Weather Service’s COSMO–DE
32 model with horizontal grid lengths of 2.8 and 1 km.
33 Both runs failed to predict the storm because simulated
34 updraughts along the convergence line were too weak
35 for parcels to overcome CIN. Over the next decade,
36 significant improvements in forecasting convection and its
37 associated hazards (e.g. flash flooding) are anticipated, with
38 the introduction of convective-scale ensemble prediction
39 systems (e.g. Clark *et al.* 2012) and continuing advances
40 in the assimilation of high-resolution remotely sensed
41 observations (e.g. Renshaw and Francis 2011). However,
42 in certain meteorological situations, improved prediction
43 might only be achieved with the use of even higher
44 resolutions ($\Delta x < 1$ km). Of course, the computational
45 requirements for such configurations are vast, and in
46 the near future, resources may be better spent on other
47 modelling developments, such as those mentioned above.
48
49 Thus, for the current generation of high-resolution NWP
50 models, efforts may be required to refine the treatment

of horizontal diffusion so that artificial smoothing of
convergence zones (and other sharp gradients) is minimised.

Returning to the issue of QSCSs, this study and GCM05
highlight the potential significance of quasi-stationary sea
breeze fronts as a mechanism by which convection may be
repeatedly initiated in one area. The basic ingredients for
such a feature—a positive land–sea temperature difference
and an offshore-directed wind component—are no doubt
quite common. However, the balance between the two is
delicate, as evidenced in the present case by the sudden
inland movement of the convergence line following a subtle
shift in the background flow. Based on a synthesis of many
previous numerical investigations of sea breezes, Crosman
and Horel (2010) suggested that an offshore geostrophic
wind greater than $4\text{--}8\text{ m s}^{-1}$ but less than $6\text{--}11\text{ m s}^{-1}$ could
cause a sea breeze front to stall at the coastline. However,
in the present case, the offshore wind component was only
around $1\text{--}2\text{ m s}^{-1}$. This discrepancy may be related to the
relatively small land–sea temperature difference ($1\text{--}2\text{ }^{\circ}\text{C}$),
but also to the existence of a strong along-shore wind
component. Historically, the along-shore component of
the background wind has been considered of secondary
importance to the cross-shore component which strongly
modulates the ability of the sea breeze to move inland or
even form (Crosman and Horel 2010). However, this may in
part be because the majority of numerical investigations of
these interactions have considered infinite coastlines, either
through the use of 2-dimensional models or 3-dimensional
models with periodic boundary conditions in the along-
shore direction. We hypothesise that in the case of a finite-
length coastline (e.g. a peninsula) with a strong along-
shore background wind, the sea breeze circulation will be
weaker (at least near the upstream end of the coastline)
because the offshore air is being continually replenished and
therefore cannot fully adjust to the thermally driven pressure
gradient. Thus, for a given land–sea temperature contrast,
a weaker offshore-directed background wind component
would be required to balance the sea breeze and create a
quasi-stationary convergence line.

In future work, we hope to investigate quasi-stationary stationary sea breeze fronts using a variety of high-resolution idealised simulations. Specifically, we would like to determine the region of $V_g-\Delta T$ parameter space (where V_g is the low-level geostrophic wind and ΔT is the land-sea temperature difference) for which these features can form. Currently, we are constructing a climatology of QSCSs in the UK which will provide valuable information about the frequency of these storms and their relation to coastlines and other topographic features.

Acknowledgement

R. Warren was supported through a National Environment Research Council (NERC) studentship (Reference No. NE/I528569/1) with CASE support from the Met Office. Nimrod radar data and UM analyses were provided by the British Atmospheric Data Centre (BADC), and atmospheric sounding data was provided by the University of Wyoming. We thank Maggie Summerfield, Sarah Alcock, and Suzanne Long of the Environment Agency for supplying rain gauge data and information regarding river levels, and Stephen Burt for providing the corrected Lesnewth rain gauge record. Thanks also to Willie McGinty and Emilie Carter for respectively providing the UKV and 500-m configurations of the Unified Model. Further invaluable help with the model simulations was provided by Rosalyn Hatcher, Carol Halliwell, Sylvia Bohnenstengel, Adrian Lock, and Jonathan Wilkinson. We also thank Giovanni Leoncini, Terry Davies, Simon Vosper, Stuart Webster, Steve Willington, Dan Suri, Nick Graham, Brian Golding and Roy Kershaw for helpful discussions and suggestions.

References

Barthlott C, Schipper JW, Kalthoff N, Adler B, Kottmeier C, Blyth A, Mobbs S. 2010. Model representation of boundary-layer convergence triggering deep convection over complex terrain: A case study from COPS. *Atmos. Res.* **95**(2–3): 172–185, doi: 10.1016/j.atmosres.2009.09.010.

Bryan GH, Wyngaard JC, Fritsch JM. 2003. Resolution requirements for the simulation of deep moist convection.

Mon. Weather Rev. **131**(10): 2394–2416, doi:10.1175/1520-0493(2003)131<2394:RRFTSO>2.0.CO;2.

Burt S. 2005. Cloudburst upon Hendraburnick Down: The Boscastle storm of 16 August 2004. *Weather* **60**(8): 219–227, doi:10.1256/wea.26.05.

Chappell CF. 1986. Quasi-stationary convective events. In: *Mesoscale Meteorology and Forecasting*, Ray PS (ed), American Meteorological Society: Boston, MA, pp. 289–310.

Clark AJ, Weiss SJ, Kain JS, Jirak IL, Coniglio M, Melick CJ, Siewert C, Sobash RA, Marsh PT, Dean AR, Xue M, Kong F, Thomas KW, Wang Y, Brewster K, Gao J, Wang X, Du J, Novak DR, Barthold FE, Bodner MJ, Levit JJ, Entwistle CB, Jensen TL, Correia J. 2012. An overview of the 2010 Hazardous Weather Testbed Experimental Forecast Program spring experiment. *B. Am. Meteorol. Soc.* **93**(1): 55–74, doi:10.1175/BAMS-D-11-00040.1.

Crosman ET, Horel JD. 2010. Sea and lake breezes: A review of numerical studies. *Bound.-Lay. Meteorol.* **137**(1): 1–29, doi:10.1007/s10546-010-9517-9.

Davies T, Cullen MJP, Malcolm AJ, Mawson MH, Staniforth A, White AA, Wood N. 2005. A new dynamical core for the Met Office's global and regional modelling of the atmosphere. *Q. J. R. Meteorol. Soc.* **131**(608): 1759–1782, doi:10.1256/qj.04.101.

Davis RS. 2001. Flash flood forecast and detection methods. In: *Severe Convective Storms, Meteorological Monographs*, vol. 28, Doswell CA (ed), American Meteorological Society: Boston, MA, pp. 481–525.

Doswell CA. 1987. The distinction between large-scale and mesoscale contribution to severe convection: A case study example. *Weather Forecast.* **2**(1): 3–16, doi:10.1175/1520-0434(1987)002<0003:TDBLSA>2.0.CO;2.

Doswell CA, Brooks HE, Maddox RA. 1996. Flash flood forecasting: An ingredients-based methodology. *Weather Forecast.* **11**(4): 560–581, doi: 10.1175/1520-0434(1996)011<0560:FFFAIB>2.0.CO;2.

Ducrocq V, Nuissier O, Ricard D, Lebeaupin C, Thouvenin T. 2008. A numerical study of three catastrophic precipitating events over southern France. II: Mesoscale triggering and stationarity factors. *Q. J. R. Meteorol. Soc.* **145**(630): 131–145, doi:10.1002/qj.199.

Edwards JM, Slingo A. 1996. Studies with a flexible new radiation code. I: Choosing a configuration for a large-scale model. *Q. J. R. Meteorol. Soc.* **122**(531): 689–719, doi:10.1002/qj.49712253107.

Essery RLH, Best MJ, Betts RA, Cox PM, Taylor CM. 2003. Explicit representation of subgrid heterogeneity in a GCM land surface scheme. *J. Hydrometeorol.* **4**(3): 530–543, doi:10.1175/1525-7541(2003)004<0530:EROSHI>2.0.CO;2.

Golding B. 2005. Boscastle and north Cornwall post flood event study: Meteorological analysis of the conditions leading to flooding on 16 August 2004. Technical report, Met Office. Forecasting Research Technical Report No. 459.

- 1
2
3 Golding B, Clark P, May B. 2005. The Boscastle flood: Meteorological
4 analysis of the conditions leading to flooding on 16 August 2004.
5 *Weather* **60**(8): 230–235, doi:10.1256/wea.71.05.
6
7 Golding BW. 1998. Nimrod: A system for generating automated
8 very short range forecasts. *Meteorol. Appl.* **5**(1): 1–16, doi:
9 10.1017/S1350482798000577.
10
11 Gregory D, Rowntree PR. 1990. A mass flux convection scheme
12 with representation of cloud ensemble characteristics and stability-
13 dependent closure. *Mon. Weather Rev.* **118**(7): 1483–1506, doi:
14 10.1175/1520-0493(1990)118<1483:AMFCSW>2.0.CO;2.
15
16 Hand WH. 2005. Climatology of shower frequency in the British Isles at 5
17 km resolution. *Weather* **60**(6): 153–158, doi:10.1256/wea.129.04.
18
19 Jones CD, Macpherson B. 1997. A latent heat nudging scheme for the
20 assimilation of precipitation data into an operational mesoscale model.
21 *Meteorol. Appl.* **4**(3): 269–277, doi:10.1017/S1350482797000522.
22
23 Lean HW, Clark PA, Dixon M, Roberts NM, Fitch A, Forbes R, Halliwell
24 C. 2008. Characteristics of high-resolution versions of the Met Office
25 Unified Model for forecasting convection over the United Kingdom.
26 *Mon. Weather Rev.* **136**(9): 3408–3424, doi:10.1175/2008MWR2332.1.
27
28 Leoncini G, Plant RS, Gray SL, Clark PA. 2012. Ensemble forecasts of
29 a flood-producing storm: Comparison of the influence of model-state
30 perturbations and parameter modifications. *Q. J. R. Meteorol. Soc.* doi:
31 10.1002/qj.1951.
32
33 Lock AP, Brown AR, Bush MR, Martin GM, Smith RNB. 2000. A
34 new boundary layer mixing scheme. Part I: Scheme description and
35 single-column model tests. *Mon. Weather Rev.* **128**(9): 3187–3199, doi:
36 10.1175/1520-0493(2000)128<3187:ANBLMS>2.0.CO;2.
37
38 Maddox RA, Chappell CF, Hoxit LR. 1979. Synoptic and meso- α scale
39 aspects of flash flood events. *B. Am. Meteorol. Soc.* **60**(2): 115–123,
40 doi:10.1175/1520-0477-60.2.115.
41
42 Maddox RA, Hoxit LR, Chappell CF, Caracena F. 1978. Comparison
43 of meteorological aspects of the Big Thompson and Rapid City
44 flash floods. *Mon. Weather Rev.* **106**(3): 375–389, doi:10.1175/1520-
45 0493(1978)106<0375:COMAOT>2.0.CO;2.
46
47 Miglietta MM, Regano A. 2008. An observational and numerical study of a
48 flash-flood event over south-eastern Italy. *Nat. Hazard Earth Sys.* **8**(6):
49 1417–1430, doi:10.5194/nhess-8-1417-2008.
50
51 Miller STK, Keim BD, Talbot RW, Mao H. 2003. Sea breeze:
52 Structure, forecasting, and impacts. *Rev. Geophys.* **41**(3): 1011, doi:
53 10.1029/2003RG000124.
54
55 Monk GA. 1987. Topographically related convection over the British Isles.
56 In: *Satellite and Radar Imagery Interpretation*, Bader M, Waters A
57 (eds), Preprints for a workshop held at Reading, 20–24 July 1987.
58 EUMETSAT: Darmstadt, Germany, pp. 305–324.
59
60 Petersen WA, Carey LD, Rutledge SA, Kniviel JC, Johnson RH,
Doesken NJ, McKee TB, Vonder Haar T, Weaver JF. 1999. Mesoscale
and radar observations of the Fort Collins flash flood of 28 July
1997. *B. Am. Meteorol. Soc.* **80**(2): 191–216, doi:10.1175/1520-
0477(1999)080<0191:MAROOT>2.0.CO;2.
Renshaw R, Francis PN. 2011. Variational assimilation of cloud fraction
in the operational Met Office Unified Model. *Q. J. R. Meteorol. Soc.*
137(661): 1963–1974, doi:10.1002/qj.980.
Roberts NM, Lean HW. 2008. Scale-selective verification of rainfall
accumulations from high-resolution forecasts of convective events.
Mon. Weather Rev. **136**(1): 78–97, doi:10.1175/2007MWR2123.1.
Romero R, Doswell CA, Ramis C. 2000. Mesoscale numerical study of
two cases of long-lived quasi-stationary convective systems over eastern
Spain. *Mon. Weather Rev.* **128**(11): 3731–3751, doi:10.1175/1520-
0493(2001)129<3731:MNSOTC>2.0.CO;2.
Schumacher RS, Johnson RH. 2005. Organization and environmental
properties of extreme-rain-producing mesoscale convective systems.
Mon. Weather Rev. **133**(4): 961–976, doi:10.1175/MWR2899.1.
Schumacher RS, Johnson RH. 2008. Mesoscale processes contributing to
extreme rainfall in a midlatitude warm-season flash flood. *Mon. Weather
Rev.* **136**(10): 3964–3986, doi:10.1175/2008MWR2471.1.
Shepherd DJ, Colquhoun JR. 1985. Meteorological aspects of an
extraordinary flash flood event near Dapto, New South Wales. *Aust.
Meteorol. Mag.* **33**(2): 87–102.
Smith RNB. 1990. A scheme for predicting layer clouds and their water
content in a general circulation model. *Q. J. R. Meteorol. Soc.* **116**(492):
435–460, doi:10.1002/qj.49711649210.
Tang Y, Lean HW, Bornemann J. 2012. The benefits of the Met Office
variable resolution NWP model for forecasting convection. *Meteorol.
Appl.* doi:10.1002/met.1300.
Wilson DR, Ballard SP. 1999. A microphysically based precipitation
scheme for the UK Meteorological Office Unified Model. *Q. J. R.
Meteorol. Soc.* **125**(557): 1607–1636, doi:10.1002/qj.49712555707.
Wilson JW, Foote GB, Crook NA, Fankhauser JC, Wade CG, Tuttle
JD, Mueller CK, Krueger SK. 1992. The role of boundary-
layer convergence zones and horizontal rolls in the initiation of
thunderstorms: A case study. *Mon. Weather Rev.* **120**(9): 1785–1815,
doi:10.1175/1520-0493(1992)120<1785:TROBLC>2.0.CO;2.
Wilson JW, Schreiber WE. 1986. Initiation of convective
storms at radar-observed boundary-layer convergence lines.
Mon. Weather Rev. **114**(12): 2516–2536, doi:10.1175/1520-
0493(1986)114<2516:IOCSAR>2.0.CO;2.
Wulfmeyer V, Behrendt A, Bauer HS, Kottmeier C, Corsmeier U, Blyth A,
Craig G, Schumann U, Hagen M, Crewell S, Di Girolamo P, Flamant
C, Miller M, Montani A, Mobbs S, Richard E, Rotach MW, Arpagaus
M, Russchenberg H, Schlüssel P, König M, Gärtner V, Steinacker R,
Dorninger M, Turner DD, Weckwerth T, Hense A, Simmer C. 2008.
The Convective and Orographically induced Precipitation Study. *B. Am.
Meteorol. Soc.* **89**(10): 1477–1486, doi:10.1175/2008BAMS2367.1.

1
2
3 Zhang M, Zhang DL. 2012. Subkilometer simulation of a torrential-rain-
4 producing mesoscale convective system in east China. Part I: Model
5 verification and convective organization. *Mon. Weather Rev.* **140**(1):
6 184–201, doi:10.1175/MWR-D-11-00029.1.
7
8
9
10
11
12
13
14
15
16
17
18
19
20
21
22
23
24
25
26
27
28
29
30
31
32
33
34
35
36
37
38
39
40
41
42
43
44
45
46
47
48
49
50
51
52
53
54
55
56
57
58
59
60

For Peer Review